Contrib Mineral Petrol (2010) 159:493–519
DOI 10.1007/s00410-009-0437-y

ORIGINAL PAPER

Trace element partitioning in the granulite facies

Franziska Nehring · Stephen F. Foley · Pentti Hölttä

Received: 9 July 2008 / Accepted: 5 August 2009 / Published online: 28 August 2009

Abstract Analyses of trace elements in the mineral phases of granulites provide important information about the trace element distribution in the lower crust. Since granulites are often considered residues of partial melting processes, trace element characteristics of their mineral phases may record mineral/melt equilibria thus giving an opportunity to understand the nature and composition of melts in the lower continental crust. This study provides an extensive set of mineral trace element data obtained by LA-ICP-MS analyses of mafic and intermediate granulites from Central Finland. Mass balance calculations using the analytical data indicate a pronounced contribution of the accessory minerals apatite for the REE and ilmenite for the HFSE. Coherent mineral/mineral ratios between samples point to a close approach to equilibrium except for minerals intergrown with garnet porphyroblasts. Mineral trace element data were used for the formulation of a set of $D^{\text{mineral/melt}}$ partition coefficients that is applicable for trace element modelling under lower crustal conditions. $D^{\text{mineral/melt}}$ were derived by the application of predictive models and using observed constant mineral/mineral ratios. The comparison of the calculated $D^{\text{mineral/melt}}$ with experimental data as well as the relationship between mineral trace element contents and a leucosome with a composition close to an equilibrium melt provides additional constraints on mineral/melt partitioning. The D values derived in this study are broadly similar to magmatic partition coefficients for intermediate melt compositions. They provide a first coherent set of D values for Sc, V, Cr and Ni between clinopyroxene, amphibole, garnet, orthopyroxene, ilmenite and melt. In addition, they emphasize the strong impact that ilmenite exerts on the distribution of Nb and Ta.

Keywords Partition coefficients · Crustal melting · Granulite · LA-ICP-MS · Trace element distribution

Communicated by J. Blundy.

F. Nehring (✉) · S. F. Foley
Earth System Science Research Centre
and Institute of Geosciences, Johannes Gutenberg University,
Becher-Weg 21, 55099 Mainz, Germany
e-mail: nehring@uni-mainz.de; Franziska.Nehring@awi.de

S. F. Foley
e-mail: foley@uni-mainz.de

P. Hölttä
Geological Survey of Finland, Betonimiehenkuja 4,
02151 Espoo, Finland
e-mail: pentti.holtta@gsf.fi

Introduction

High temperature anatexis within the middle to lower crust is a direct consequence of the incongruent melting of hydrous minerals (muscovite, amphibole, biotite) leaving an anhydrous residue and generating significant amounts of granitoid melts (Brown 1994; White and Powell 2002). Granulites are often considered as the anhydrous residues of such dehydration melting processes (Harley 1989; White and Powell 2002) although local CO_2 flushing may also drive dehydration (Hansen et al. 1987; Ravindra Kumar 2004; Harlov et al. 2006). Granulites typically occur in the deeply eroded Archean proportions of the continents (see Vielzeuf and Vidal 1990 and references therein) as well as in the deep parts of younger accretionary arcs and thickened crust (Rudnick and Gao 2003 and references therein; Garrido et al. 2006).

Petrological experiments under P-T-conditions resembling natural granulite facies conditions have been

conducted in a variety of geochemical systems (Beard and Lofgren 1991; Wolf and Wyllie 1994; Patiño Douce and Beard 1995; Rapp 1995; Singh and Johannes 1996; Skjerlie and Johnston 1996; Springer and Seck 1997; Patiño Douce and Harris 1998; Sisson et al. 2005). They clarified the mineralogical assemblages, melting reactions as well as the major element composition of granulite facies minerals and melts.

The behaviour of trace elements during crustal melting has gained much less interest (Bea et al. 1994; Rudnick and Gao 2003) even though it is crucial for understanding the geochemical characteristics of crustally derived granitoid melts. Fundamental insight into trace element redistribution in the middle to lower crust can be gained by studying the mineral trace element budget in natural granulite facies rocks. Mafic and intermediate granulites from Central Finland provide excellent opportunities for in situ trace element determination by LA-ICP-MS due to their granoblastic mineral growth. They have simple mineral parageneses, containing garnet in addition to clinopyroxene, plagioclase and minor amphibole at pressures >10 kbar and orthopyroxene at lower pressures.

It is appealing to calculate the trace element composition of the anatectic melt in equilibrium with the granulitic residue using the granulite trace element budget as the residual composition. However, sets of mineral/melt partition coefficients $D^{\text{mineral/melt}}$ that were experimentally derived for granulite facies conditions for minerals in mafic source rocks in equilibrium with tonalitic-andesitic liquids, and those that exist contain a limited number of elements (Brenan et al. 1995; Klein et al. 1997, 2000; Hilyard et al. 2000; Barth et al. 2002). We try to overcome this deficit in the experimental data by using mineral compositions in the Finnish granulites for the derivation of a reliable set of partition coefficients that are useful for modelling crustal melting scenarios.

Geological setting and petrography

The samples were collected from granulite blocks cropping out within amphibolite-facies TTG gneisses between Sukeva, Iisalmi and Varpaisjärvi in Central Finland. Mafic granulites from the NW part of the area (Iisalmi–Sukeva and Varpanen area) have protolith ages of 3.1–3.2 Ga (Hölttä et al. 2000), whereas granulites from the SE (Jonsa area) are intermediate in composition and have minimum protolith ages of 2.73–2.70 Ga (Mänttäri and Hölttä 2002). The age difference between the NE and the SW granulites indicates terrane accretion during the late Archean which caused granulite metamorphism in both terranes between 2.70 and 2.63 Ga (Hölttä et al. 2000; Mänttäri and Hölttä 2002). Peak metamorphic conditions obtained from Grt–Cpx–Pl–Qtz assemblages indicate 9–11 kbar and 800–950°C. A detailed description of metamorphic reactions and determination of the P-T-path for the mafic and intermediate granulites is given in Hölttä and Paavola (2000).

Granoblastic Grt–Cpx–Pl ± Hbl assemblages are typical for the 3.1 Ga mafic granulites of the Iisalmi–Sukeva area in the NW. Single grains of prograde amphibole are enclosed by clinopyroxene or garnet while retrograde amphibole forms rims on garnet or clinopyroxene. Garnet is porphyroblastic, reaches grain sizes up to 2–3 cm, and contains inclusions of other minerals present in the host rock (mostly Cpx).

Prograde, granoblastic orthopyroxene is characteristic for the 2.7 Ga intermediate granulites of the Jonsa block. The modal mineralogy of intermediate granulites varies significantly, with plagioclase constituting 30–50%, amphibole 10–40% and clinopyroxene 10–30% of the modal abundance. Orthopyroxene is approximately half as abundant as clinopyroxene. Garnet in intermediate granulites is restricted to Fe-rich and more mafic layers. The field appearance and compositional differences within intermediate granulites suggest a pre-metamorphic layering of broadly andesitic rocks resembling volcanic successions.

Opaque phases such as ilmenite and magnetite and accessory apatite are abundant in all types of granulite. Biotite is a minor constituent of intermediate granulites only.

Analytical methods

All geochemical analyses were accomplished in the laboratories of the Department of Geosciences, Johannes Gutenberg-University, Mainz, Germany. Bulk rock analyses were performed for major and a number of trace elements (Cr, Ni, Sc, V) by XRF. All other trace elements were obtained by fusion of rock powder on an Iridium strip heater followed by analysis of the glasses by LA-ICP-MS. For further explanation of this method, see Fedorowich et al. (1993) and Nehring et al. (2008).

Major elements in minerals were analysed by JEOL JXA 8900 RL electron microprobe using wavelength dispersive analysis and a range of natural and synthetic standards. The data were corrected using the CITZAF procedure (Armstrong 1995).

In situ mineral trace element measurements were performed with an Agilent 7500ce quadrupole ICP-MS coupled with a NewWave Research UP-213 laser ablation unit. The analyses were made using Argon as plasma and carrier gas except for orthopyroxene and plagioclase which were analysed with a He/Ar mixture to increase sensitivity. Data acquisition was accomplished in a rapid, peak-jumping

mode with one point per peak at 10 ms dwell time. Before each analysis, background measurements were performed for 60 s. Plasma conditions were adjusted to oxide formation rates below 0.5% (monitored using the 248/232 mass ratio), thus no further oxide corrections were necessary. Either ^{43}Ca or ^{44}Ca were used as internal standards for amphibole, clinopyroxene, garnet, plagioclase and apatite, and Si[29] for orthopyroxene. Certified glass reference material NIST SRM 612 was the external standard and data reduction was carried out using the software "Glitter". The elemental concentrations of NIST SRM 612 used for standardization were taken from Pearce et al. (1997) except for Zr in NIST SRM 612 for which the preferred value of 38 μg/g given in the GeoReM database (http://georem.mpch-mainz.gwdg.de/) was used. Instrument performance and stability were monitored by repeated measurements of USGS reference glass BCR-2G during the analytical sessions. The precision on BCR-2G over the course of this study was better than 10% for all elements and accuracies are within 5% except for Zr, Hf and Ni (10%) (Table 1). Detection limits in the argon mode are lower than 0.05 μg/g except for Sc (0.2 μg/g), Cr (1 μg/g), Ni (0.2 μg/g), V and Ba (0.1 μg/g).

Sample description and bulk rock geochemistry

Samples numbered 02M2, 34M2, 36M1 and 140M from the Iisalmi–Sukeva area are typical grt–Cpx-granulites. Sample 36M1 contains discrete grains of prograde brown amphibole while the other samples only contain retrograde green amphibole. Mafic granulite 02M2 is distinct in containing small equally distributed garnet grains instead of large granoblastic ones. Mafic granulites have SiO_2 contents of 48–49 wt%, CaO-contents between 12 and 17 wt%, high concentrations of compatible elements (Sc, V, Ni and Cr) and exhibit LREE depletion (Table 2; Fig. 1).

Intermediate Opx–Cpx-granulites are typical for the Jonsa block in the SE part of the granulite area. Three samples were taken from granulite patches within diatexite (80M, 102a, 114M) and two further samples stem from coarse grained granulite bodies, several metres wide (76a, 112M). The intermediate granulites characteristically have low contents of compatible elements. They are LREE enriched with $(La/Yb)_N$ between 3.5 and 6. On spidergrams, they exhibit negative Nb–Ta and Zr–Hf anomalies.

One garnet-bearing sample (76M1) was additionally collected in the Jonsa area, taken from the border of a thick

Table 1 LA-ICP-MS results for USGS reference glass BCR-2G compared to preferred values

	Mean ± SD (μg/g)	RSD (%)	Accuracy (%)	GeoReM (μg/g)
BCR-2G				
Sc	33.0 ± 1.5	5	100	33 ± 2
V	413 ± 28	7	97	425 ± 18
Cr	16.6 ± 2.1	12	98	17 ± 2
Ni	11.9 ± 1.0	9	91	13 ± 2
Rb	44.9 ± 3.9	9	95	47 ± 0.5
Sr	330 ± 8	2	97	342 ± 4
Ba	669 ± 27	4	98	683 ± 43
Y	30.8 ± 1.4	4	88	35 ± 3
Zr	167 ± 12	7	91	184 ± 15
Hf	4.30 ± 0.27	6	89	4.84 ± 0.28
Nb	12.6 ± 0.4	3	101	12.5 ± 1
Ta	0.79 ± 0.04	5	102	0.78 ± 0.06
La	24.4 ± 0.9	3	99	24.7 ± 0.3
Ce	51.6 ± 1.4	3	97	53.3 ± 0.5
Nd	28.0 ± 0.9	3	97	28.9 ± 0.3
Sm	6.41 ± 0.29	4	97	6.59 ± 0.07
Eu	1.90 ± 0.06	3	97	1.97 ± 0.02
Gd	6.24 ± 0.36	6	93	6.71 ± 0.07
Dy	6.10 ± 0.39	6	95	6.44 ± 0.06
Er	3.44 ± 0.22	6	93	3.7 ± 0.04
Yb	3.32 ± 0.20	6	98	3.39 ± 0.03
Lu	0.48 ± 0.04	8	97	0.5 ± 0.01

CaO as internal standard, measured as ^{43}Ca. NIST SRM 612 was the external calibrator for BCR-2G. Preferred values for BCR-2G are taken from the GeoReM database

Table 2 Bulk rock major-oxide and trace element data for studied samples (values in italics by XRF, other trace elements by LA-ICP-MS)

	Grt–Cpx-granulites (Iisalmi – Sukeva)				Grt–Cpx- gran. (Varpanen)		Opx–Cpx–(Grt)- granulites (Jonsa)					Leucosome
	02M2	34M2	36M1	140M	12M1	49M	76M1	76a	80M	112M	114M	36L2
SiO_2	48.1	49.2	48.4	48.4	50.3	49.5	55.7	52.4	55.0	52.1	60.0	64.3
TiO_2	0.81	1.15	1.32	0.77	1.56	1.50	1.04	0.45	0.43	0.40	0.60	1.08
Al_2O_3	15.6	15.8	13.7	14.9	16.1	13.1	13.6	15.7	15.0	15.9	17.3	16.2
Fe_2O_3	11.5	12.9	16.0	10.9	11.8	17.1	13.7	9.0	9.1	8.5	6.1	5.14
MnO	0.31	0.32	0.25	0.22	0.18	0.23	0.17	0.16	0.16	0.15	0.09	0.08
MgO	5.23	5.43	8.8	6.54	5.53	6.47	3.78	7.98	6.17	7.62	3.1	2.1
CaO	15.2	12.8	11.7	16.8	9.56	8.59	8.00	11.7	8.50	11.7	6.77	5.38
Na_2O	2.14	1.8	1.23	1.46	3.55	2.99	2.93	2.46	3.75	3.03	4.73	4.16
K_2O	0.11	0.09	0.09	0.05	0.24	0.62	0.7	0.26	1.25	0.30	1.06	0.72
P_2O_5	0.04	0.04	0.07	0.04	0.39	0.12	0.12	0.04	0.05	0.07	0.13	0.51
Total	99.0	99.5	101.6	100.1	98.7	100.1	99.6	100.1	99.4	99.7	99.7	100.5
Sc	*45*	*53*	*60*	*43*	*32*	*48*	*36*	*37*	*22*	*35*	*13*	8
V	*263*	*353*	*405*	*243*	*218*	*370*	*263*	*161*	*115*	*151*	*125*	83
Cr	*294*	*338*	*221*	*397*	*37*	*130*	*b.d.*	*16*	*228*	*7*	*18*	78
Ni	*176*	*173*	*112*	*189*	*71*	*75*	*11*	*49*	*153*	*50*	*26*	41
Rb	1.02	1.46	1.11	0.67	0.40	1.99	1.01	0.42	25.3	0.89	5.77	6.00
Sr	131	100	59	116	444	262	309	268	282	271	467	342
Y	18.5	26.1	28.3	10.8	23.7	29.8	20.2	8.45	14.3	8.39	12.6	10.0
Zr	30.9	17.7	22.5	20.4	43.7	22.3	55.1	17.2	8.90	14.6	20.2	292
Nb	1.52	1.98	2.01	1.26	5.24	4.28	4.24	1.27	3.55	1.25	4.16	6.90
Ba	27.5	18.6	7.88	13.6	194	218	233	58.2	452	91.6	174	239
La	1.91	1.15	0.90	1.69	15.8	7.16	16.7	4.99	12.0	5.85	10.8	22.8
Ce	6.55	5.01	3.54	5.48	35.0	19.0	37.5	11.7	24.7	12.5	25.0	52.2
Pr	1.11	0.86	0.71	0.88	4.70	2.76	4.56	1.56	3.04	1.60	3.56	6.68
Nd	5.96	5.43	4.48	4.71	22.0	13.5	18.8	6.55	11.1	6.58	15.8	26.0
Sm	1.91	2.20	1.96	1.53	4.90	3.88	3.92	1.53	2.43	1.44	3.20	4.67
Eu	0.73	0.86	0.69	0.61	1.87	1.26	1.12	0.57	0.71	0.55	0.93	1.06
Gd	2.52	3.40	3.20	1.82	5.05	4.86	3.95	1.50	2.31	1.50	2.66	3.60
Dy	3.21	4.68	4.90	2.06	4.55	5.56	3.54	1.60	2.20	1.65	2.30	1.83
Er	2.11	3.27	3.30	1.20	2.47	3.38	1.93	0.95	1.31	0.92	1.29	0.71
Yb	2.17	3.40	3.51	1.31	2.23	3.20	1.67	0.97	1.47	0.98	1.24	0.56
Lu	0.33	0.52	0.52	0.18	0.33	0.47	0.24	0.16	0.22	0.14	0.19	0.09
Hf	1.03	0.80	0.86	0.69	1.12	1.20	1.66	0.68	0.37	0.66	0.78	8.23
Ta	0.10	0.11	0.11	0.08	0.25	0.29	0.20	0.09	0.19	0.07	0.31	0.25

Additionally, the composition of a leucosome from outcrop 36 is given, which was used in the calculations of mineral/melt partition coefficients

stromatic leucosome. The skeletal garnet from this sample is intergrown with plagioclase and quartz suggesting growth in a melt-rich environment. The sample is LREE-enriched and has very low Cr and Ni contents.

Two grt–Cpx-granulites (12M1 and 49M) from the central part of the area (Varpanen area) were studied. They are only slightly richer in SiO_2 and Na_2O and poorer in CaO than mafic granulites from the Iisalmi area in the NW but their REE abundances closely resemble intermediate granulites from Jonsa area (Fig. 1).

Mineral chemistry

Amphibole

Only amphibole inferred from textural criteria to be prograde was analysed by LA-ICP-MS. Prograde amphiboles are ferropargasitic, pargasitic and edenitic in composition (after Leake 1997) with only minor in-sample variation (Appendix 1). An exception is sample 36M1 where amphibole enclosed in garnet has higher X_{Mg} than larger

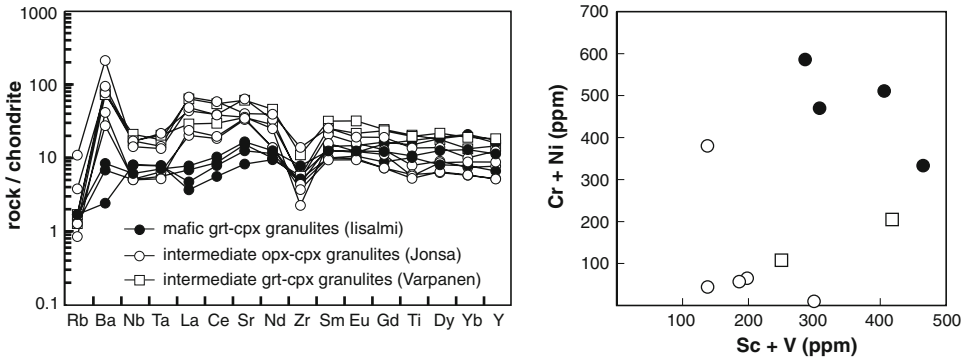

Fig. 1 Bulk rock trace element pattern of granulites. Note the clear distinction between intermediate granulites and mafic granulites. LREE-enrichment, negative Nb–Ta anomalies and low contents of compatible elements in intermediate granulites could be related to an arc-setting of the precursor rocks. Contrasting with this are the geochemical features of mafic granulites which resemble tholeiitic basalts

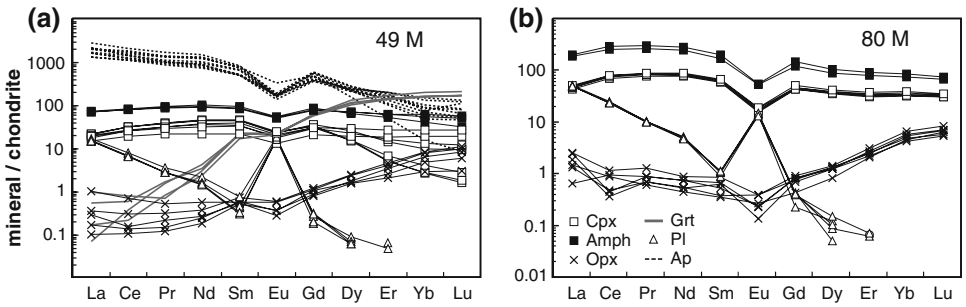

Fig. 2 Examples of trace element patterns of mineral phases from mafic (**a**) and intermediate (**b**) granulites. Note the spread in HREE-contents in clinopyroxene from sample 49M and the enrichment in REE as well as the strong negative Eu anomaly in sample 80M from a diatexite outcrop

amphibole grains lacking contact with garnet. Compared to amphibole in thick granulite bodies with low K_2O (0.64–0.85 wt%) contents, amphiboles from granulite patches within diatexite (80M, 102a, 114M) are enriched in K_2O (1.5–1.8 wt%). HREE depletion occurs in amphibole enclosed in garnet and in amphibole from garnet-bearing sample 76M1. REE are markedly enriched and a strong negative Eu-anomaly appears in amphibole from granulite patches in diatexite outcrops (Fig. 2b).

Amphibole in mafic granulite 36M1 has very low Ba, Rb and Sr contents of <14, <4 and 20–40 ppm, respectively (Appendix 2). High Ba and Sr in amphibole are observed in garnet-bearing samples 12M1, 76M1 and 49M while enrichment of Rb occurs in amphibole from the granulite patches within diatexite (80M, 102a and 114M).

The variability of Cr, Ni, Sc and V contents in amphibole from the different settings is attributed to the different petrological origin of the precursor rocks. Amphibole is the major host for Nb and Ta after ilmenite and rare biotite.

Clinopyroxene

Clinopyroxene is mainly augite and diopside with X_{Mg} between 0.6 and 0.8 (Appendix 1). No systematic variation in X_{Mg} between mafic and intermediate granulites was observed.

Clinopyroxene REE patterns are very similar to those of amphibole in the same sample but the absolute amount of REE is 2–4 times lower. A similar distribution between amphibole and clinopyroxene is also observed for V, Cr, Ni, Sr, Y, Th and U. Contents of Sc, Zr and Hf are equal in amphibole and clinopyroxene but contents of Rb, Ba, Nb and Ta are much lower in clinopyroxene (Appendix 2). Clinopyroxene intergrown with garnet porphyroblasts exhibit depletion from Gd to Lu while clinopyroxene in the matrix further away from the porphyroblasts has flat HREE patterns (Fig. 2a). All clinopyroxene is HREE depleted in samples 02M2 and 140M.

Orthopyroxene

Orthopyroxene has X_{Mg} of 0.5–0.7. Its overall low content of trace elements (Appendix 2) suggests limited control of orthopyroxene on the trace element budget except for the transition metals. REE contents in Opx increase with increasing atomic number, with HREE contents less than 10 times the chondritic value (Fig. 2).

Garnet

Garnet has X_{Alm} 0.5–0.62, X_{Prp} 0.13–0.33 and X_{Grs} 0.15–0.28. REE contents in garnet strongly increase with atomic

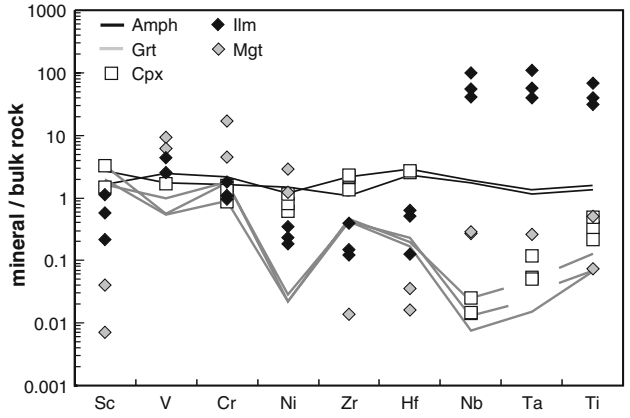

Fig. 3 Comparison of trace element contents in ilmenite and magnetite to contents in major mineral phases. Averaged values of the individual mineral phases are displayed and only samples in which ilmenite and magnetite were analysed are used (12M2, 36M1 and 140M). Nb and Ta are strongly enriched in ilmenite while V, Cr and Ni show preference for magnetite

number (Appendix 2) except for garnet in sample 34M2 which exhibits decreasing contents of HREE from Dy to Lu. While the MREE contents are consistent within one sample, LREE as well as HREE exhibit some variations. The LREE are commonly below detection limits but sample 36M1 shows that especially La and Ce contents can be quite variable. In addition to the strong influence on the HREE, garnet contributes significantly to the Sc, V, Cr and Y budget (Fig. 3).

Plagioclase

Plagioclase in mafic granulites has X_{An} 0.53–0.7 in correspondence with the CaO-rich bulk composition. Plagioclase from the two wide granulite bodies 76a and 112M have X_{An} of 0.47–0.53 while plagioclase elsewhere in intermediate granulites has X_{An} of 0.26–0.33. The most sodic plagioclase occurs in granulite patches within diatexite.

Plagioclase is strongly enriched in Sr and also contains high amounts of Ba (Appendix 2). Plagioclase LREE contents exhibit little variation within one sample. They are strongly fractionated with $La_N/Sm_N = 10–60$ and a prominent positive Eu-anomaly is developed in all samples (Fig. 2). HREE contents in plagioclase commonly lie below the detection limits of LA-ICP-MS.

Apatite

Apatite occurs as small euhedral crystals enclosed in plagioclase and along grain boundaries between plagioclase and other minerals. Apatite grains are larger and more abundant in granulites from the Varpanen and Jonsa block, where bulk rock P_2O_5 contents are higher (Table 2). Due to the small grain size, apatite was only analysed in samples 12M1 and 49M. Apatites from both samples show little variation in major elements with CaO 54–56 wt% and P_2O_5 40–42 wt%. Halogen contents are made up exclusively of fluorine ($\sim$3 wt%) in sample 49M while sample 12M1 contains 0.4–0.8 wt% chlorine in addition to $\sim$2 wt% fluorine.

LA-ICP-MS analyses show that apatite incorporates high amounts to the REE as well as Th and U (Appendix 2). Sample 12M1 shows increased compatibility of Nd, Sm and Gd compared to La and Ce while in sample 49M the chondrite-normalised pattern slightly decreases from La to Sm (Fig. 2a). Both samples exhibit negative Eu-anomalies, which are more pronounced in sample 49M.

Ilmenite and magnetite

Oxide phases are abundant in all groups of granulites. Ilmenite and magnetite occur together as irregularly formed blebs with rounded grain boundaries. Broad lamellae of ilmenite in magnetite are observed in sample 76M1 suggesting exsolution of the phases upon cooling. Oxides were analysed for major elements in several samples but grains large enough for analysis by LA-ICP-MS were only found in samples 12M1, 36M1 and 140M.

Ilmenites consist of 50–53 wt% TiO_2, 45–48 wt% FeO (Appendix 1) and contain less than 1 wt% MgO and MnO. The TiO_2 content of magnetite is <0.5 wt%. Both minerals contain significant amounts of V, Cr and Ni but only ilmenite shows affinity towards the High Field Strength Elements (HFSE) and incorporates Sc, Nb and Ta as well as small amounts of Zr (Fig. 3; Appendix 2).

Discussion

Evidence for partial melting in the Finnish granulites and the significance of leucosomes

All of the granulite lithologies contain tonalitic leucosomes, but leucosomes are more abundant in intermediate granulites where they form stromatic layers compared to thin veins and patches of leucosome in mafic granulites. Leucosomes are considered as remnants of a melt phase that was produced by dehydration melting reactions in the mafic and intermediate source rocks. Peak mineral assemblages and textures suggest that mafic granulites from the Iisalmi–Sukeva area formed by the following general dehydration-melting reaction (Wolf and Wyllie 1994; Hartel and Pattison 1996):

$$\text{Amph} + \text{Pl} \pm \text{Qtz} = \text{Cpx} + \text{Grt} + \text{Melt} \quad (1)$$

Meanwhile, melt, clinopyroxene and orthopyroxene instead of garnet formed by reaction 2 (Patiño Douce and Beard 1995) in intermediate granulites from the Jonsa and Varpanen area.

$$\text{Amph} + \text{Qtz} = \text{Pl} + \text{Cpx} + \text{Opx} + \text{Melt} + \text{Ox} \quad (2)$$

Reactions 1 and 2 are typical breakdown reactions of amphibole leading to the formation of a leucocratic melt phase and an anhydrous granulitic residue, reaction 2 being favoured at lower pressures and elevated SiO_2-activities. Evidence for both reactions can be drawn from the occurrence of amphibole inclusions in pyroxenes and garnet in mafic granulites and from the common overgrowth of pyroxenes on amphibole in intermediate granulites (Fig. 4).

The degree of melting in mafic granulites was 10–30% as can be inferred using a batch melting model and amphibolites from Central Finland as source rocks (Nehring et al. 2009). The modal abundances of pyroxenes versus amphibole in intermediate granulites suggest that the melt fraction in these rocks may have not exceeded 10% and that the reaction progress was likely restricted by the availability of quartz (Nehring et al. 2009). Simple batch melting models indicate that such low melt fractions will leave the LREE in intermediate granulites largely unaffected. In contrast, low contents of U, Th and the Large Ion Lithophile Elements (LILE) in the examined granulites may have been caused by the fluid mobile behaviour of these elements during metamorphism (Jacob and Foley 1999, Zack and John 2007).

The common preservation of granulite facies mineral assemblages apart from retrograde reactions along fractures or along the rims of leucosomes points to the loss of much of the melt produced by reactions 1 and 2 (White and Powell 2002). However, we find evidence for melt accumulation and melt metasomatism in the granulite patches within diatexite. We suggest that elevated SiO_2 of the bulk rock sample 114M, elevated K_2O in amphibole and Na_2O in plagioclase as well as REE-enrichment in amphibole and clinopyroxene from the granulite patches result from metasomatism by the melt-rich host.

Although leucosomes provide important evidence of partial melting, their composition usually does not match a typical melt composition. The characteristic geochemical features of most leucosomes, e.g. high SiO_2 contents and low REE contents with prominent positive Eu anomalies are more consistent with the crystallization of plagioclase and quartz along melt migration pathways (Marchildon and Brown 2001; Solar and Brown 2001; Nehring et al. 2009). Thus, leucosomes may give evidence for the presence of a melt phase at peak metamorphism although they do not reflect the actual melt composition. Nevertheless, among the many leucosome samples we analysed, few leucosomes with lower SiO_2 and elevated REE contents have been found (Nehring et al. 2009). Among others a leucosome

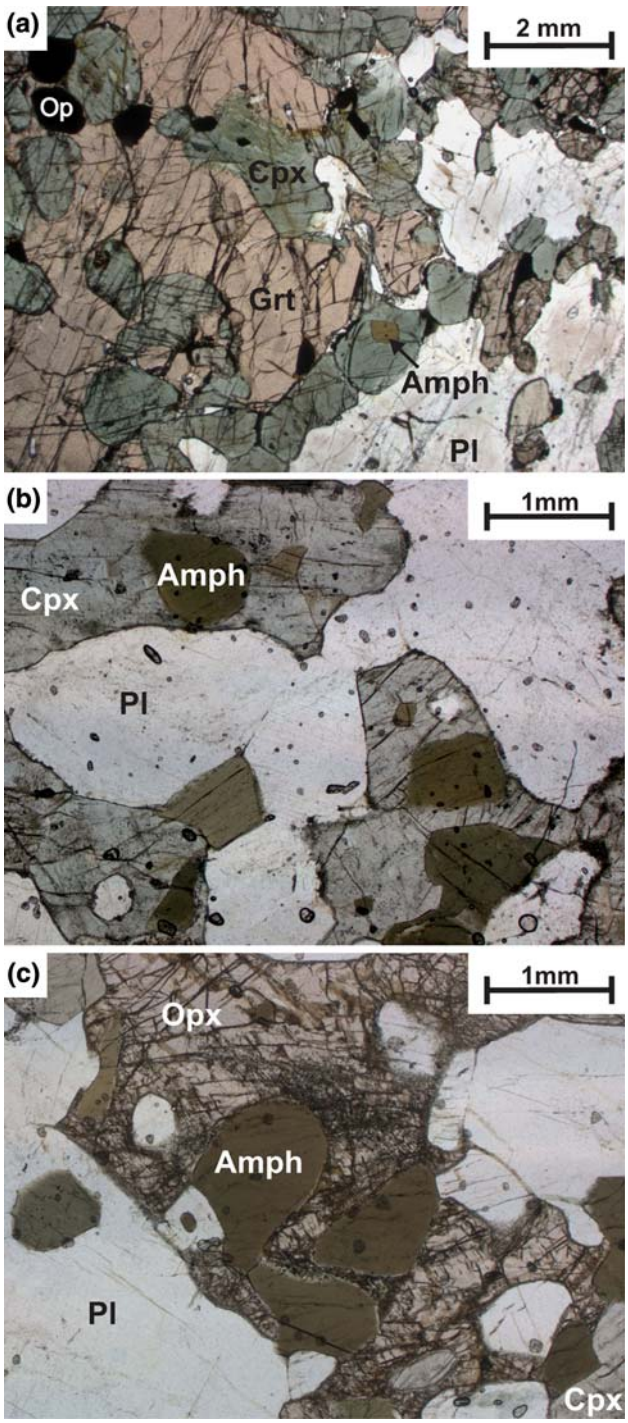

Fig. 4 **a** Garnet porphyroblast intergrown with clinopyroxene in sample 49M. Pay attention to the abundance of opaque phases and the amphibole inclusion in clinopyroxene. Clinopyroxene (**b**) and orthopyroxene (**c**) overgrowth on amphibole in intermediate granulite 112M

(36L2), found at outcrop 36, may represent a largely unmodified melt batch. It has moderate SiO_2 of 64.3 wt% and exibits a smooth decrease in the REE pattern without any significant Eu or Sr anomaly (Table 2). Its trace element composition can be modelled by about 20% partial melting of an amphibolite leaving a garnet-bearing residue (Nehring et al. 2009). We therefore take the composition of this specific leucosome as a proxy for the melt composition derived by partial melting processes that left the mafic granulites as residues.

Mass balance calculations and attainment of equilibrium

Mass balance calculations were performed in order to see whether the trace element budget of the samples is hosted by the major mineral phases alone or if accessory phases contribute significantly to the trace element budget. Villaseca et al. (2003) observed that accessory phases are sparse in lower crustal granulites and that major phases incorporate high amounts of trace elements. They inferred that a major redistribution of trace elements between accessory and major mineral phases takes place during granulite facies metamorphism.

Modal mineralogy (Table 3) was estimated by least squares fitting based on the major element composition of the bulk rock and the mineral compositions obtained by microprobe analysis. Point counting either overestimates or underestimates the amount of garnet in mafic granulites depending on the presence or absence of large granoblastic garnet grains in thin sections. The addition of quartz is necessary for samples that experienced pronounced melt/rock interaction, e.g. samples from granulite patches within diatexite (114M, 80M) and sample 76M1 which was taken from the rim of a thick leucosome. No mass balance calculations were undertaken for sample 36M1 because it contains a high amount of Opx–Pl-symplectites between garnet porphyroblasts and clinopyroxene.

The presence of an additional REE-rich phase is required to fulfil mass balances for the REE in most granulites (Fig. 5). Apatite is an important carrier of the REE and it has been observed especially in LREE-rich intermediate granulites. We used the concentration of phosphorus as a proxy for the abundance of apatite in the samples. A strong improvement of the mass balances for the REE is observed by including apatite (taking the composition as measured in sample 49M) in the calculations.

Table 3 Modal abundances of minerals in granulites calculated from least squares calculations and point counting (sample 102a)

Sample	Sample type	Sample area	Amph	Cpx	Opx	Pl	Kfs	Grt	Qtz	Bt	Mgt	Ilm	Ap	Total
02 M2	Grt–Cpx-granulite	Iisalmi–Sukeva	3	39	–	45	–	10	–	–	1	1	0.1	100
34 M2	Grt–Cpx-granulite	Iisalmi–Sukeva	4	30	–	45	–	17	–	–	1	2	–	99
140M	Grt–Cpx-granulite	Iisalmi–Sukeva	–	52	–	41	–	5	–	–	1	1	0.1	100
12 M1	Grt–Cpx-granulite	Varpanen	5	20	12	55	–	1	–	1	4	1	1.0	100
49M	Grt–Cpx-granulite	Varpanen	18	20	12	36	–	7	–	2	3	1	0.3	99
76 M1	Grt–Cpx-granulite	Jonsa	30	10	–	33	–	8	15	1	3	–	0.3	100
76 a	Opx–Cpx-granulite	Jonsa	18	19	12	50	–	–	1	–	0.1	0.08	0.1	100
80M	Opx–Cpx-granulite	Jonsa	3	20	17	50	5	–	2	2	0.1	0.5	0.1	100
102a	Opx–Cpx-granulite	Jonsa	30	4	3	59	–	–	3	–	1	–	–	100
112M	Opx–Cpx-granulite	Jonsa	20	23	8	48	–	–	–	–	0.3	0.05	0.1	100
114M	Opx–Cpx-granulite	Jonsa	15	10	5	55	5	–	9	–	0.5	0.5	0.4	100

No calculations were attempted for sample 36M1 due to its high abundance of symplectites

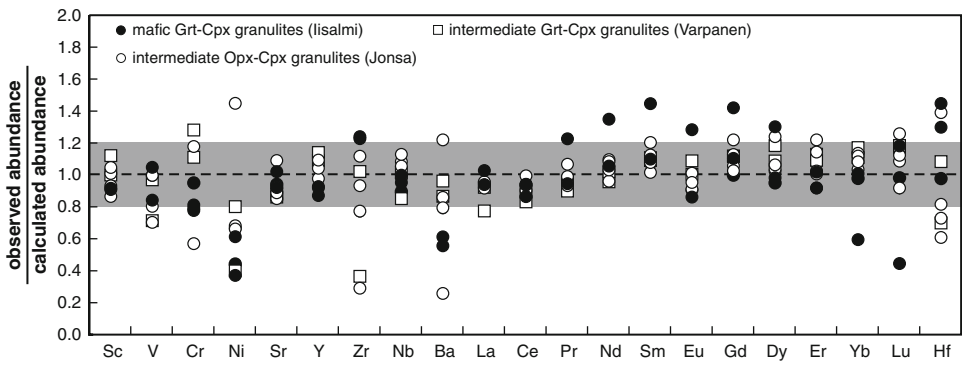

Fig. 5 Results of mass balance calculations by least squares fittings for the trace element budget in granulite samples. Good results are obtained for the REE except Iisalmi sample 34M2. Poor fits of Ni, Zr, Ba and Hf are attributed to the neglect of pyrite/chalcopyrite, zircon and potassic feldspar in the calculations

The concentrations of V, Cr and Ni strongly depend on the amount and composition of magnetite and ilmenite. Ni is often underestimated by up to 50%. This suggests that Ni may be hosted in an additional phase such as pyrite or chalcopyrite, which have been detected optically in most samples but were not analysed due to the small grain size. The overestimation of Ni by the mass balance calculations in sample 76M1 is attributed to the low whole rock Ni content in this sample lying close to the detection limit of XRF. Apart from some poor fits of Zr and Ba that can be attributed to the neglect of zircon and potassic feldspar in the calculations, the mass balance calculations indicate that no further accessory minerals are required to fulfil mass balances, pointing to a rather simple mineral assemblage in mafic and intermediate granulites.

Mineral/mineral ratios are constant among the samples indicating a close approach to equilibrium despite their variable composition (Table 4). Within mafic granulites, amphibole and clinopyroxene closely associated with garnet show HREE depletion as can be expected by equilibration with HREE-absorbing garnet while mineral grains further away from the garnet porphyroblasts have flat HREE pattern. The most plausible explanation for the variation of the mineral REE contents within one sample is a lack of equilibrium between garnet and the bulk matrix. Garnet probably started to grow after most of the clinopyroxene already formed. Slow diffusion of REE through the matrix (Skora et al. 2006) may have prevented equilibration so that garnet could only seize REE from its immediate surroundings. The extent of disequilibrium between garnet and whole rock volume may strongly vary between the samples due to the size and distribution of the garnet porphyroblast. For instance, the well equilibrated assemblage in sample 02M2 with an overall HREE depletion in clinopyroxene may have been favoured by small but equally distributed garnet grains. For further considerations the apparent disequilibrium between garnet and the matrix also demands very careful calculation of mineral/mineral ratios in mafic granulites from minerals belonging to the same equilibration volume, e.g. minerals having equilibrated with garnet or not.

Derivation of a set of mineral/melt partition coefficients

The aim of this study is to provide a set of mineral/melt partition coefficients ($D_{\mathrm{i}}^{\mathrm{mineral/melt}}$) that is applicable for modelling partial melting processes of mafic and intermediate source rocks under middle and lower crustal conditions. Petrological experiments conducted in this pressure–temperature range often do not provide trace element data at all (Rushmer 1991; Beard and Lofgren 1991; Patiño Douce and Beard 1995) or consider only a limited number of trace elements and minerals (Brenan et al. 1995; Klein et al. 1997; Hill et al. 2000; Hilyard et al. 2000; Xiong 2006). It is therefore appealing to compile a set of $D_{\mathrm{i}}^{\mathrm{mineral/melt}}$ that reflects the observed trace element ratios in the granulite facies mineral assemblages considered in this study.

One way to derive $D_{\mathrm{i}}^{\mathrm{mineral/melt}}$ is to use the predictive model for crystal-melt partitioning given by Blundy and Wood (1994). The model is based on the Brice (1975) equation, which relates the partition coefficient of element *i* (D_i) to that of element *o* (D_o), where the latter has the same ionic radius r_o as the crystallographic site of interest:

$$D_i = D_o \exp\left(\frac{-4\pi E N_A\left[\frac{r_o}{2}(r_i - r_o)^2 + \frac{1}{3}(r_i - r_o)^3\right]}{RT}\right).$$

N_A is Avogadro's number, E is the Young's Modulus of the crystallographic site, R is the gas constant and T is the temperature in K.

Wood and Blundy (1997) refined this model for REE-partitioning between clinopyroxene and anhydrous silicate melt incorporating pressure and temperature as well as compositional effects. Klein et al. (1997, 2000) undertook similar approaches for amphibole and van Westrenen et al. (2001) for garnet. Wood and Blundy (2002) considered the influence of melt water content on clinopyroxene-melt partitioning. Their findings may also apply for the samples considered here as will be shown in the next section. Using the predictive models we can calculate $D_{\mathrm{REE}}^{\mathrm{Cpx/melt}}$ and afterwards we may derive $D_{\mathrm{REE}}^{\mathrm{mineral/melt}}$ by using the observed $D_{\mathrm{REE}}^{\mathrm{mineral/Cpx}}$. For reference, we compared $D_{\mathrm{REE}}^{\mathrm{mineral/melt}}$ with published data as well as the data we got from the mineral/leucosome ratio from outcrop 36. This approach allows us to conclude whether the leucosome 36L2 indeed represents an unmodified melt batch and if it may also be used for the derivation of $D_{\mathrm{i}}^{\mathrm{mineral/melt}}$ for elements other than the REE.

In addition, we carefully included other models linking mineral/melt partitioning to the major element composition of the minerals. We used the relationship between amphibole Mg#, amphibole Ti-content and $D_{\mathrm{Nb/Ta}}^{\mathrm{Amph/melt}}$ (Tiepolo et al. 2000), the incorporation of Zr into amphibole as a function of Ti and Al contents on the amphibole M2 site (Dalpé and Baker 2000) or the dependance of $D_{\mathrm{Sr}}^{\mathrm{Pl/melt}}$ on the anorthite content of plagioclase (Bédard 2006; Bindeman et al. 1998). All of the calculated $D_{\mathrm{i}}^{\mathrm{mineral/melt}}$ have been compared to published values thereby confirming their credibility, leading to a comprehensive set of partitioning coefficients, which clearly reflects the trace element distribution observed in middle to lower crustal granulites.

Amphibole/clinopyroxene REE-partitioning

The trivalent REE partition into the crystal-chemically analogous eightfold M4-site in amphibole and the M2-site

Table 4 Mineral/mineral ratios of trace elements in granulite samples

Amphibole/clinopyroxene

	12M1	36M		49M	76a	76M1		80M	102a	112M	114M
		HREE				HREE					
		Low	High			Low	High				
Sr	2.9	4.1	3.9	4.5	3.4 (22)	3.9	4.0	2.9	2.7 (14)	1.9 (56)	3.0 (24)
Sc	0.8	1.1	1.1	1.0	0.9 (10)	1.0	0.8	1.0	0.7 (32)	1.1 (17)	0.7 (10)
V	1.3	–	1.9	1.4	2.0 (7)	1.9	1.9	–	1.7 (12)	2.4 (10)	1.7 (12)
Cr	1.0	3.7	2.0	1.7	2.4 (28)	1.4	1.1	3.4	1.6 (37)	3.1 (56)	1.2 (30)
Ni	1.8	2.3	1.6	1.7	2.3 (7)	1.5	1.6	1.9	1.7 (12)	2.5 (14)	1.6 (14)
Y	2.2	3.9	2.8	3.2	3.4 (12)	3.7	3.1	2.7	2.8 (18)	3.5 (12)	2.8 (10)
Zr	0.8	1.1	0.9	0.9	1.0 (27)	1.2	0.9	1.0	1.3 (24)	1.2 (19)	1.2 (15)
Hf	0.9	1.2	1.1	0.9	–	1.3	1.0	–	1.2 (30)	–	1.2 (14)
La	3.0	2.9	3.1	3.7	3.3 (16)	4.7	4.2	4.1	5.3 (16)	3.4 (13)	4.2 (12)
Ce	2.5	2.5	3.1	3.1	3.0 (14)	3.6	3.6	3.6	4.2 (14)	3.2 (7)	3.6 (16)
Pr	2.5	2.3	2.9	3.0	3.0 (17)	3.6	3.4	3.4	3.9 (13)	3.2 (9)	3.6 (19)
Nd	2.4	2.5	3.0	2.8	3.0 (10)	3.7	3.2	3.2	3.8 (8)	3.2 (12)	3.4 (16)
Sm	2.2	2.7	2.9	2.6	3.2 (29)	3.5	3.0	2.9	3.2 (15)	3.1 (23)	3.2 (29)
Eu	2.5	2.5	3.3	2.9	2.9 (19)	3.3	3.2	3.1	2.9 (13)	3.2 (18)	3.3 (17)
Gd	2.3	2.6	3.1	2.8	3.2 (18)	3.5	2.9	2.9	3.0 (20)	3.4 (15)	3.1 (19)
Dy	2.1	3.3	3.0	2.8	3.0 (19)	3.4	3.0	2.5	2.8 (19)	3.3 (14)	2.7 (16)
Er	1.9	4.3	2.7	3.1	3.4 (21)	4.1	3.0	2.5	2.6 (21)	3.3 (14)	2.8 (12)
Yb	1.8	4.2	2.3	3.0	3.2 (19)	2.6	3.1	2.3	2.3 (15)	3.2 (17)	2.3 (19)
Lu	2.0	4.7	2.5	2.8	2.8 (23)	2.1	2.6	2.1	2.1 (14)	3.3 (22)	2.0 (13)

Garnet/clinopyroxene

	02M2	12M1 cpx in grt	34M2 Low HREE	36M Low HREE	49M Low HREE	76M1 Low HREE	140M
Sc	0.89 (11)	1.5 (4)	1.2 (5)	1.1	0.83	1.1	1.1 (17)
V	0.47 (10)	0.41 (8)	n.a.	0.40	0.40	0.61	0.59 (21)
Cr	2.3 (25)	1.4 (16)	1.2 (44)	1.5	1.9	1.9	–
Ni	0.02 (11)	0.03 (51)	0.03 (18)	0.04	0.02	0.05	0.02 (51)
Y	26 (26)	14 (14)	11 (55)	15	17	35	33 (38)
Zr	0.14 (34)	0.21 (17)	0.20 (27)	0.20	0.20	0.24	0.20 (14)
Hf	0.05 (20)	0.09 (19)	0.05 (27)	0.07	0.05	0.07	0.07 (45)
Pr	0.04 (16)	0.03 (32)	0.03 (26)	–	0.03	0.03	–
Nd	0.12 (14)	0.08 (13)	0.08 (19)	0.08	0.08	0.1	0.08 (30)
Sm	0.74 (14)	0.40 (15)	0.43 (18)	0.49	0.47	0.75	0.55 (29)
Eu	1.7 (12)	0.89 (18)	1.0 (15)	0.94	0.96	1.4	1.3 (20)
Gd	3.0 (14)	1.6 (16)	1.6 (19)	1.8	1.9	3.1	2.3 (11)
Dy	12 (19)	6.1 (5)	6.5 (37)	6.8	7.5	14.0	11 (23)

Orthopyroxene/clinopyroxene

	49M	76a	80M	102a	112M	114M
Sc	0.24 (36)	0.19 (4)	0.17 (25)	0.16 (43)	n.a.	0.13 (11)
V	0.23 (35)	0.30 (5)	n.a.	0.18 (8)	n.a.	0.16 (35)
Cr	0.39 (89)	–	0.39 (54)	0.16 (33)	n.a.	0.42 (34)
Ni	1.07 (27)	1.20 (10)	1.04 (30)	1.00 (15)	n.a.	1.10 (17)
Eu	0.02 (32)	–	0.02 (44)	0.01 (33)	–	–

Table 4 continued

Orthopyroxene/clinopyroxene

	49M	76a	80M	102a	112M	114M
Gd	0.04 (17)	0.03 (50)	0.02 (29)	0.01 (20)	0.03 (10)	–
Dy	0.08 (22)	0.04 (47)	0.03 (24)	0.03 (46)	0.04 (40)	0.04 (39)
Er	0.18 (31)	0.09 (36)	0.07 (21)	0.06 (47)	0.09 (46)	0.10 (14)
Yb	0.35 (37)	0.20 (33)	0.15 (24)	0.16 (42)	0.21 (19)	0.20 (27)
Lu	0.45 (42)	0.27 (36)	0.20 (22)	0.20 (39)	0.28 (42)	0.26 (23)

plagioclase/clinopyroxene

	02M2	12M1	34M2	36M	49M	61M	76a	76M1	102a	112M	114M	140M
Sr	37 (15)	35 (38)	44 (32)	51 (39)	39 (17)	37 (34)	40 (16)	37 (16)	40 (13)	28 (32)	44 (17)	42 (20)
La	1.1 (21)	0.9 (26)	1.2 (37)	1.4 (18)	0.8 (19)	1.2 (31)	1.5 (13)	0.9 (34)	1.1 (15)	1.2 (18)	1.2 (9)	1.3 (34)
Ce	0.34 (20)	0.27 (24)	0.36 (29)	0.43 (21)	0.26 (25)	0.41 (27)	0.50 (13)	0.27 (37)	0.32 (25)	0.41 (12)	0.36 (14)	0.42 (34)
Pr	0.14 (19)	0.11 (23)	0.15 (24)	0.18 (20)	0.09 (30)	0.16 (33)	0.19 (14)	0.10 (36)	0.11 (25)	0.19 (31)	0.13 (20)	0.15 (33)
Nd	0.08 (25)	0.05 (24)	0.08 (26)	0.09 (23)	0.04 (38)	0.11 (42)	0.10 (15)	0.05 (44)	0.05 (16)	0.10 (29)	0.06 (19)	0.07 (41)
Sm	0.02 (25)	0.02 (27)	0.02 (41)	0.03 (38)	0.01 (59)	–	0.04 (59)	0.02 (42)	0.01 (18)	–	–	0.03 (44)
Eu	0.96 (20)	0.45 (31)	0.73 (23)	0.64 (25)	0.84 (25)	0.50 (23)	0.60 (20)	0.79 (29)	0.55 (22)	0.69 (33)	0.61 (15)	0.90 (33)

Plagioclase/amphibole

	12M1	36M	49M	61M	76a	76M1	80M	102a	112M	114M
Sr	12	10	9.2	11 (27)	12 (7)	9.4 (10)	14	15 (8)	12 (11)	15 (22)
Ba	1.1	1.0	1.1	1.1 (18)	1.5 (5)	0.8 (25)	1.0	–	1.8 (13)	1.0 (36)

Apatite/clinopyroxene

	12M1	49M
Sr	11 (15)	12 (21)
Y	6.1 (25)	10 (63)
La	–	89 (31)
Ce	–	53 (34)
Pr	–	36 (36)
Nd	–	29 (43)
Sm	8.7 (40)	18 (42)
Eu	7.3 (27)	9.2 (30)
Gd	8.3 (30)	16 (34)
Dy	5.5 (22)	9.7 (37)
Er	5.0 (26)	
Yb	3.6 (23)	
Lu	3.6 (31)	

Ilmenite/clinopyroxene

	36M	12M1	140M
Sc	0.38 (77)	0.35 (32)	0.15 (47)
V	1.7 (47)	3.4 (15)	1.5 (34)
Cr	1.0 (70)	0.68 (54)	1.4 (23)
Ni	0.31 (69)	0.29 (28)	0.19 (25)

Ilmenite/amphibole

	12M1	36M
Nb	32	21
Ta	50	29

Only ratios for elements clearly above the detection limits are given. Values in brackets are the relative standard deviation (RSD [%]) within one sample calculated from $RSD_{mineral\ A} + RSD_{mineral\ B}$. No RSD% is given if less than 4 grains of one of the minerals were analysed for instance due to the low abundance of amphibole in mafic granulites. No ratios are given in the case of extensive scattering of the concentrations of an element in a specific mineral

in clinopyroxene where they substitute for Ca (Bottazzi et al. 1999). Observed $D_{REE}^{Amph/Cpx}$ are 2–5 using mineral pairs that are in textural equilibrium with one another. This agrees with $D_{REE}^{Amph/Cpx}$ found by Schröter (2006) in a granulite facies mafic sill from East Antarctica and with values reported by Storkey et al. (2005) from a metabasite of the Arunta block, Australia. Pride and Muecke (1981) reported $D_{REE}^{Amph/Cpx} \sim 2$ for granulites from the Scourian

Complex in Scotland. $D_{REE}^{Amph/Cpx} > 3$ were also reported by Witt-Eickschen and Harte (1994) for peridotite xenoliths from the East-Eifel.

In contrast, $D_{REE}^{Amph/Cpx} \sim 1$ has regularly been reported from ultramafic rocks, including xenoliths of pyroxenite (Zack et al. 1997), hornblendite (Orejana et al. 2006), lherzolite (Chazot et al. 1996) and peridotite (Ionov and Hofmann 1995; Glaser et al. 1999). Witt-Eickschen and Harte (1994) claim that incorporation of the REE into clinopyroxene increases as its Na-content increases because of a more flexible behaviour of the M2-site at higher Na-contents. In addition, Hill et al. (2000) observed a positive correlation between the incorporation of the HFSE and, to a lesser extent, the REE into clinopyroxene with increasing CaTs-component in clinopyroxene. Clinopyroxene from the Finnish granulites characteristically has a lower jadeite component as well as lower CaTs-component compared to clinopyroxenes for which $D_{REE}^{Amph/Cpx} \sim 1$ has been reported (Fig. 6) explaining the low incorporation of the REE into clinopyroxene from the studied samples.

We applied the Wood and Blundy (1997) equations to the clinopyroxene composition observed in the Finnish granulites. This yields reasonable results for the optimum radius of the REE-hosting lattice site $r_0^{3+} = 1.03$ Å and for the Young's modulus $E_x^{3+} = 284$ GPa at 900°C and 10 kbar. However, the calculations for the strain free partition coefficient (D_0^{3+}) for the M2 site yield values between 2 and 3 which are high compared to experimentally derived D_0^{3+} in similar systems that range between 0.6 and 2 (Green and Pearson 1985; Hill et al. 2000; Klein et al. 2000; Barth et al. 2002). The overestimation of D_0^{3+} in clinopyroxene could be due to the effect of H_2O on crystal-melt partitioning of trace elements (Wood and Blundy 2002), which suppresses the activities of all other components in the melt. Partial melts produced by amphibole-dehydration melting will be hydrous. If the corrections for melt H_2O-contents given in Wood and Blundy (2002) are used, about 6 wt% H_2O in the melt are required to suppress the mean calculated anhydrous $D_0^{3+} \sim 2.6$ to a value of 1.3 which is in better agreement with experimental data. This concurs with melt H_2O-contents between 3 and 10 wt% observed in dehydration melting experiments on amphibolites (Beard and Lofgren 1991; Sen and Dunn 1994; Patiño Douce and Beard 1995). However, since firm constraints on H_2O-contents of melts from the Finnish granulites are lacking, the experimentally derived $D_0^{Cpx} = 1.05$ from Klein et al. (2000) was used for the calculation of D_i for granulites. The calculated $D_{REE}^{Cpx/melt}$ (Table 5) are higher than published values for clinopyroxene in equilibrium with basaltic melts (Hauri et al. 1994; Hart and Dunn 1993) but lower than values from Barth et al. (2002) for eclogitic minerals in equilibrium with tonalitic melt (Fig. 7a). They are in accordance with elemental ratios calculated from clinopyroxene and leucosome 36L2 from outcrop 36. This leucosome also allows direct determination of $D_{REE}^{Cpx/melt}$ by using the observed $D_{Eu}^{Cpx/leucosome} = 0.74$ for the estimation of D_0^{3+}. A lower $D_0^{3+} = 0.86$ and therefore slightly decreased $D_{REE}^{Cpx/melt}$ are obtained by this calculation (Table 5).

$D_{REE}^{Amph/melt}$ were calculated using the lattice site parameters for amphibole given in Klein et al. (1997). In their experiments, D_0^{3+} in amphibole decreases from 2.66 at 800°C to 2.29 at 850°C and 1.7 at 900°C. The low temperature $D_0^{3+} \sim 2.66$ is more likely to apply for our dataset since it meets our observation of $D_{REE}^{Amph/melt} \sim 3 * D_{REE}^{Cpx/melt}$ (Table 5). Using the observed $D_{Eu}^{Amph/leucosome} \sim 1.8$ to calculate D_0^{3+} gives slightly lower values for $D_{REE}^{Amph/melt}$ than would be expected by the mineral/mineral ratio. Nevertheless, $D_{REE}^{Amph/melt}$ calculated here agree well with $D_{REE}^{Amph/melt}$ from low temperature experiments with andesitic–tonalitic melt composition (Nicholls and Harris 1980; Sisson 1994; Klein et al. 1997; Hilyard et al. 2000) (Fig. 7b).

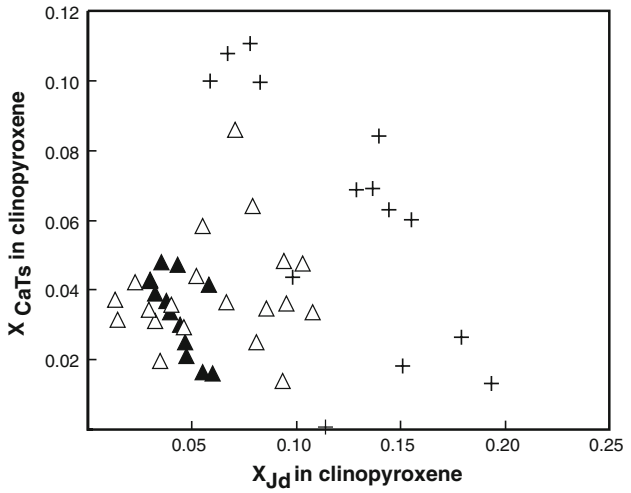

Fig. 6 CaTs and Jd components in clinopyroxene calculated after Cawthorn and Collerson (1974). Crosses are for clinopyroxenes for which $D_{REE}^{amph/cpx} \sim 1$ have been reported (see text for references). Triangles are for clinopyroxenes with $D_{REE}^{amph/cpx} > 1$ (*black triangles* this study, *white triangles* references, see text). The diagram indicates tha REE partitioning into clinopyroxene seems to be favoured by high Jd and high CaTs components

Garnet/Clinopyroxene REE-partitioning

As already discussed, garnet porphyroblasts failed to equilibrate with the whole rock volume in most of the samples. Thus, the approach of calculating $D_{REE}^{Grt/melt}$ from $D_{REE}^{Cpx/melt} \times D_{REE}^{Grt/Cpx}$ is only adopted for the two garnet-bearing mafic granulites that show rather coherent REE concentrations in clinopyroxene and garnet throughout the sample (samples 02M2 and 140M). But even among the samples 02M2 and 140M, with an overall depletion of

Table 5 Mineral/melt partition coefficients for the REE

Mineral	Input parameters	La	Ce	Nd	Sm	Eu	Gd	Dy	Er	Yb	Lu
Cpx	$D_0^{3+} = 1.05$ (taken from Klein et al. 2000) $E_X^{3+} = 284\ GPa$ (after Wood & Blundy 1997) $r_0^{3+} = 1.03 \pm 0.005$ Å (after Wood & Blundy 1997)	**0.13** (0.02)	**0.25** (0.03)	**0.50** (0.04)	**0.79** (0.04)	**0.90** (0.04)	**0.99** (0.03)	**1.10** (0.01)	**0.97** (0.02)	**0.84** (0.03)	**0.77** (0.04)
	$D_0^{3+} = 0.86 \pm 0.04$ (calculated from $D_{Eu}^{Cpx/leucosome} = 0.74$) $E_X^{3+} = 284\ GPa$ (after Wood & Blundy 1997) $r_0^{3+} = 1.03$ Å (after Wood & Blundy 1997)	0.11	0.20	0.41	0.65	0.74	0.81	0.86	0.80	0.69	0.63
	Clinopyroxene/leucosome	0.04	0.09	0.26	0.59	0.74	0.89	1.23	0.83	0.44	0.29
Amph	$D_i^{Amph/melt} = 3 \times D_i^{Cpx/melt}$	**0.40**	**0.74**	**1.5**	**2.4**	**2.7**	**3.0**	**3.1**	**2.9**	**2.5**	**2.3**
	$D_0^{3+} = 2.0$ (calculated from $D_{Eu}^{Amph/leucosome} = 1.8$) $E_X^{3+} = 200\ GPa$ (taken from Klein et al. 2000) $r_0^{3+} = 1.03$ Å (taken from Klein et al. 2000)	0.41	0.65	1.1	1.6	1.8	1.9	2.0	1.9	1.7	1.6
	Amphibole/leucosome	0.11	0.22	0.64	1.6	1.8	2.3	4.0	3.5	1.8	1.3
Opx	$D_i^{Opx/melt} = D_i^{Cpx/melt} * Opx/Cpx$	–	–	–	–	**0.02**	**0.02**	**0.03**	**0.09**	**0.16**	**0.19**
Pl	$D_i^{Pl/melt} = D_i^{Cpx/melt} * Pl/Cpx$	**0.15**	**0.09**	**0.04**	**0.03**	**0.63**	**0.02**	–	–	–	–
	Plagioclase/leucosome	0.05	0.04	0.02	0.02	0.47	0.02	–	–	–	–
Grt	$D_0^{3+} = 25 \pm 5$ (calculated from $D_{Eu}^{Grt/melt} = D_{Eu}^{Cpx/melt} = 0.9$) $E_X^{3+} = 573 \pm 16\ GPa$ (after van Westrenen et al. 2001) $r_0^{3+} = 0.95 \pm 0.002$ Å (after van Westrenen et al. 2001)	–	–	**0.09** (0.01)	**0.58** (0.01)	**0.90**	**2.2** (0.1)	**6.1** (0.6)	**12** (2)	**18** (3)	**20** (4)
	Garnet/leucosome	–	–	0.02	0.28	0.69	1.6	8.4	18	27	26
Ap	$D_i^{Ap/melt} = D_i^{Cpx/melt} * Ap/Cpx$ (minimum and maximum values calculated using variable ap/cpx ratios from sample 049M)	**11** **16**	**12** **17**	**13** **19**	**13** **18**	**8** **13**	**14** **17**	**10** **11**	**8** **9**	**4.0** **5.5**	**3.3** **4.6**

Preferred values are given in bold numbers. Values in brackets are 1 standard deviation. Values of mineral/leucosome composition from outcrop 036 are given for comparison with the calculated mineral/melt partition coefficients

HREE in clinopyroxene, strongly variable $D_{Yb}^{Grt/melt}$ of 68 and 140, respectively, are obtained.

Because of the uneven distribution of the REE in garnet and clinopyroxene, we considered it better to bracket $D_{REE}^{Grt/melt}$ by experimental data and elastic strain calculations. Since $D_{Eu}^{Cpx/Grt} \sim 1$ in all samples (Table 4), we can assume that $D_{Eu}^{Grt/melt}$ equals $D_{Eu}^{Cpx/melt} = 0.9$. This relationship can be used together with $r_0^{3+} = 0.95$ Å and $E_x^{3+} \sim 570$ GPa, calculated with the van Westrenen et al. (2001) model, because these variables only depend on garnet composition. Feeding the variables into the Brice equation yields $D_{REE}^{Grt/melt}$ that are within the range of data in tonalitic melt systems from Klein et al. (2000), Barth et al. (2002) and Xiong (2006). They are also consistent with the ratio between garnet in sample 36M1 and the leucosome composition from the same outcrop (Fig. 8a).

REE partitioning into orthopyroxene

REE contents in orthopyroxene strongly increase from the LREE to the HREE. Because LREE contents in Opx often lie below the detection limits of LA-ICP-MS only the REE

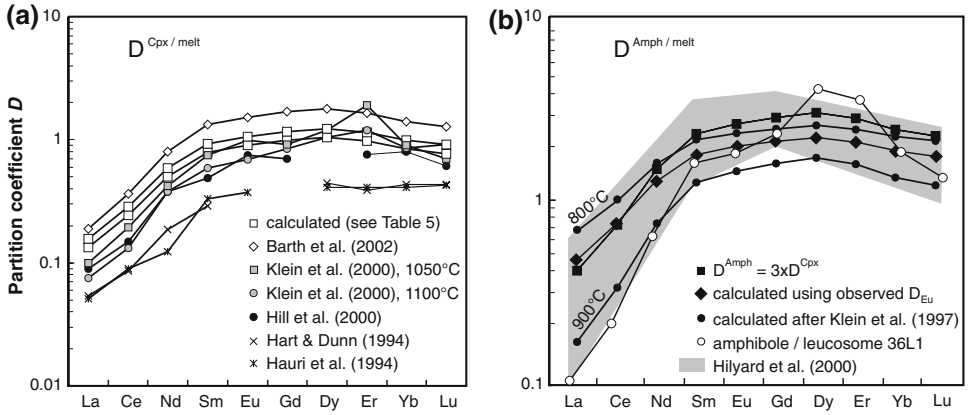

Fig. 7 REE mineral melt partition coefficients for clinopyroxene and amphibole. **a** Calculated $D_{\mathrm{REE}}^{\mathrm{Cpx/melt}}$ were derived by applying the predictive model of Wood & Blundy (1997). Slightly lower $D_{\mathrm{REE}}^{\mathrm{Cpx/melt}}$ are obtained by using the observed Eu-partitioning between clinopyroxene and leucosome 36L2. Values for tonalitic melts (Barth et al. 2002; Klein et al. 2000), andesitic melts (Hill et al. 2000) and basaltic melts (Hart and Dunn 1993; Hauri et al. 1994) are given for comparison. **b** $D_{\mathrm{REE}}^{\mathrm{Amph/melt}}$ calculated as $3 * D_{\mathrm{REE}}^{\mathrm{Cpx/melt}}$ yields values comparable to the low temperature (800°C) experiments by Klein et al. (1997). Calculations using $D_{\mathrm{Eu}}^{\mathrm{Amph/melt}}$ as a proxy for D_0^{3+} as well as E_{X}^{3+} and r_0^{3+} from Klein et al. (1997) gives values intermediate between the 800°C and 900°C experiments and are consistent with values from Hilyard et al. (2000) experimentally derived at 900–940°C and 2–5 kbar

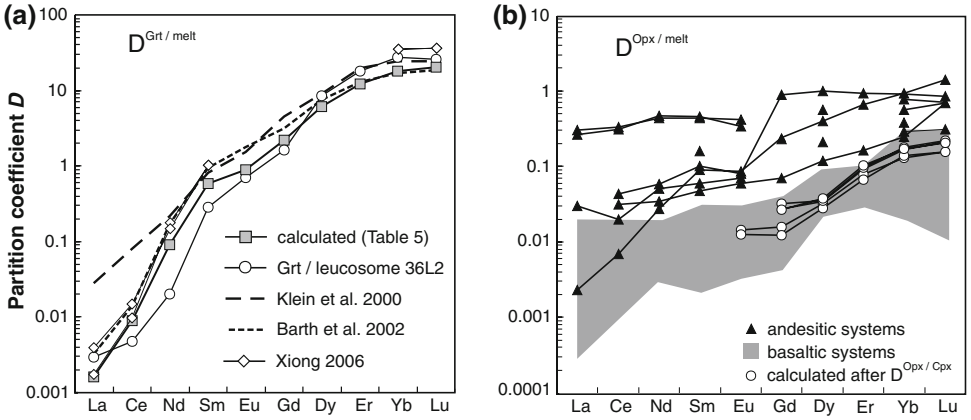

Fig. 8 REE mineral melt partition coefficients for garnet and orthopyroxene. **a** $D_{\mathrm{Eu}}^{\mathrm{Grt/melt}} = 0.9$ from the garnet/leucosome ratio of outcrop 36 together with $E_{\mathrm{X}}^{3+} = 570$ GPa and $r_0^{3+} = 0.95$ Å calculated according to van Westrenen et al. (2001) were applied for the derivation of $D_{\mathrm{REE}}^{\mathrm{Grt/melt}}$. Experimental $D_{\mathrm{REE}}^{\mathrm{Grt/melt}}$ for tonalitic melts given by Klein et al. (2000) for 900°C and 15 kbar, by Barth et al. (2002) for 1000–1040°C and 18 kbar and Xiong (2006) for 900–1100°C and 10–20 kbar are shown for comparison. **b** $D_{\mathrm{REE}}^{\mathrm{opx/melt}}$ calculated from the observed Opx/Cpx ratio are low and coincide rather with values known from basaltic than from intermediate systems

between Gd and Lu are considered further. For these elements orthopyroxene/clinopyroxene ratios increase from ~0.03 to ~0.3 (Table 4). Similar partition coefficients between Opx and Cpx are known from different geological settings, for instance from exsolution lamella of Opx in Cpx in peridotites (Hellebrand et al. 2005). REE-contents in orthopyroxene presented here are lower than values reported for other granulite localities (Pride and Muecke 1981; Schröter et al. 2004; Clarke et al. 2007). As a consequence, $D_{\mathrm{REE}}^{\mathrm{Opx/melt}}$ calculated as $D_{\mathrm{REE}}^{\mathrm{Cpx/melt}} \times D_{\mathrm{REE}}^{\mathrm{Opx/Cpx}}$ are low with for instance $D_{\mathrm{Lu}}^{\mathrm{Opx/melt}} \sim 0.20$ (Table 5). Our values for $D_{\mathrm{REE}}^{\mathrm{Opx/melt}}$ (Fig. 8b) are comparable to partition coefficients determined for basaltic systems (Irving and Frey 1984; Colson et al. 1988; McKenzie and O'Nions 1991; Cawthorn 1996; Schwandt and McKay 1998) but lower than those for andesites (Schnetzler and Philpotts 1970; Luhr and Carmichael 1980; Bacon and Druitt 1988; Nielsen et al. 1992; Dunn and Sen 1994). No comparison with leucosome 36L2 was attempted since orthopyroxene is not a member of the peak metamorphic mineral assemblage in this outcrop.

REE partitioning into plagioclase

REE partitioning into plagioclase has not been studied extensively but increasing $D_{\mathrm{REE}}^{\mathrm{Pl/melt}}$ with decreasing anorthite-content are expected from natural and experimental data (Bédard 2006). Both La and Eu concentrations in

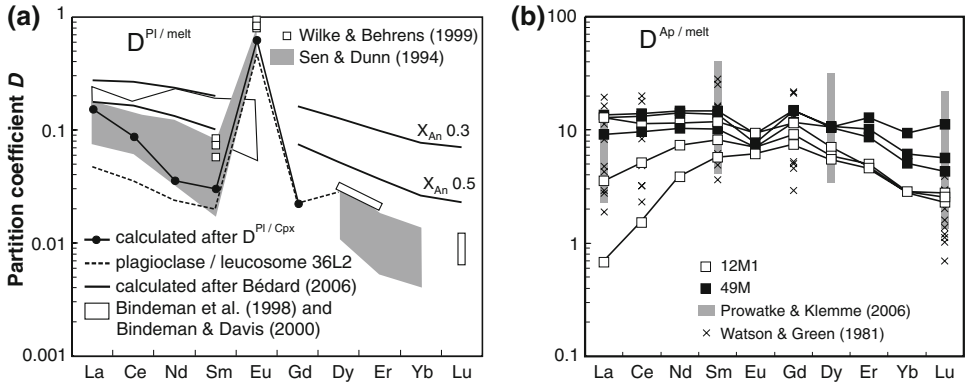

Fig. 9 REE mineral melt partition coefficients for plagioclase and apatite. **a** $D_{REE}^{Pl/melt}$ were calculated using the plagioclase/clinopyroxene ratio and the plagioclase/leucosome ratio. This approach precludes a dependence of $D_{REE}^{Pl/melt}$ on X_{An} in plagioclase as suggested by Bédard (2006). The values are lower than those calculated after Bédard (2006), Bindeman and Davis (2000) and Bindeman et al. (1998) but are in good agreement with values from Dunn and Sen (1994) experimentally derived in basaltic to andesitic systems at 1 bar and 1,100–1,200°C. Also shown is the Sm and Eu partitioning after Wilke & Behrens (1999) for a haplotonalitic melt at 850°C, 5 kbar and log fO_2 controlled at the Ni-NiO buffer. **b** REE contents in both apatite and clinopyroxene are variable and therefore different $D_{REE}^{Ap/Cpx}$ can be calculated for one sample. Accordingly, $D_{REE}^{Ap/melt}$ calculated as $D_{REE}^{Ap/Cpx}$ multiplied by $D_{REE}^{Cpx/melt}$ are variable but broadly fall into the range of values from Prowatke & Klemme (2006) and Watson & Green (1981). The spread in $D_{REE}^{Ap/melt}$ from both references is explained by increasing partitioning into apatite with evolving melt compositions

plagioclase are similar to concentrations in clinopyroxene from the same sample, with $D_{La}^{Pl/Cpx} = 1.14 \pm 0.19$ and $D_{Eu}^{Pl/Cpx} = 0.69 \pm 0.15$ (Fig. 9a). The ratio of plagioclase/clinopyroxene (Table 4) was used to determine $D_{REE}^{Pl/melt}$ from the calculated $D_{REE}^{Cpx/melt}$ (Table 5). Partition coefficients for the LREE calculated from the observed $D_{REE}^{Pl/Cpx}$ are clearly lower than predicted by Bédard (2006) or given in the extensive study of Bindeman and Davis (2000). Nevertheless, our data are consistent with values given in Dunn and Sen (1994) for basaltic and andesitic systems (Fig. 9a). Furthermore, we find good agreement with the data given in Wilke and Behrens (1999). Partitioning of Eu into plagioclase depends on the redox state of the system during partial melting since incorporation of Eu^{2+} into plagioclase is strongly preferred over incorporation of Eu^{3+}. The degree of enrichment of Eu over Sm in plagioclase from our rocks is similar to the data from Wilke and Behrens (1999) determined at 850°C and at log $fO_2 \sim -12$, close to the Ni–NiO buffer, which are reasonable conditions for granulite facies metamorphism (Rollinson and Windley 1980; Harlov 2000).

The role of apatite

Apatite incorporates high amounts of the REE via the substitutions $REE^{3+} + Si^{4+} \leftrightarrow Ca^{2+} + P^{5+}$ and $REE^{3+} + Na^{+} \leftrightarrow 2Ca^{2+}$ (Rønsbo 1989). Experimental work by Watson and Green (1981) and Prowatke and Klemme (2006) as well as studies of natural occurrences (Nagasawa 1970; Paster et al. 1974; Luhr et al. 1984; Fujimaki 1986; Mahood and Stimac 1990; Sha and Chappell 1999) demonstrated the influence of melt composition on REE partitioning into apatite. They showed that partition coefficients for the REE and other highly charged cations increase with increasing degree of polymerisation of the melt.

The apatite/clinopyroxene ratio was used to calculate $D_{REE}^{Ap/melt}$ (Table 5). For sample 12M1, this attempt is hindered by variable LREE contents which may actually be an analytical problem due to the small grain size of apatite. Sample 49M contains variable HREE contents in both clinopyroxene and apatite. Still, steadily sloping $D^{Ap/melt}$ for the HREE and a pronounced negative Eu anomaly in the $D_{REE}^{Ap/melt}$ pattern can be seen in both samples. Experimentally derived $D_{REE}^{Ap/melt}$ are rare. Nevertheless, our data fall into the range of experimental partition coefficients for basaltic andesites (Prowatke and Klemme 2006; Watson and Green 1981) (Fig. 9b).

Partitioning of the High Field Strength Elements (HFSE)

Zr and Hf follow Ti in the analogous M1-site in clinopyroxene and the M2-site in amphibole where they are involved in the local charge balance of tetrahedral Al (Tiepolo et al. 2000). In agreement with this are the observed $D^{Amph/Cpx} \sim 1$ for Zr and Hf (Table 4). Partition coefficients for Zr in amphibole are calculated using the equation given by Dalpé and Baker (2000) that relates Zr partitioning to the Ti and Al contents on the M2 site. Their model gives a mean $D_{Zr}^{Amph/melt} = 0.17$ which is in excellent agreement with the amphibole/leucosome ratio from samples 36M1/36L2 (0.15–0.18). It is however lower than experimentally derived values in tonalitic–andesitic

systems (Brenan et al. 1995; Klein et al. 1997; Hilyard et al. 2000) which are mainly 0.26–0.9. There are two likely explanations for this difference. First, the equation of Dalpé and Baker (2000) is suitable for upper mantle conditions (15–25 kbar, 1,200°C) and may not give satisfactory results for lower crustal conditions. Second, we detected inherited zircons by cathodoluminescence in leucosomes from outcrop 36 which raise the Zr content of the leucosome bulk composition above the Zr content of the equilibrium melt phase leading to decreased $D_{Zr}^{Amph/melt}$. Slightly higher $D_{Zr}^{Amph/melt}$ between 0.2 and 0.3 may therefore be more appropriate for equilibrium conditions, which are supported by findings of Hill et al. (2000) and Klein et al. (2000).

In terms of chondrite-normalised values, $Hf_N \sim 1.5 - 2.5 \times Zr_N$ in amphibole and clinopyroxene, in agreement with $D_{Hf}^{mineral/melt} > D_{Zr}^{mineral/melt}$ for both amphibole and clinopyroxene (Brenan et al. 1995; Klein et al. 1997, 2000; Hill et al. 2000; Dalpé and Baker 2000; Hilyard et al. 2000; Xiong 2006). This is also supported by $D_{Hf}^{Amph/leucosome} = D_{Hf}^{Cpx/leucosome} \sim 0.3$ compared to the above-mentioned partition coefficients for Zr of 0.15–0.18. The Hf partition coefficient is slightly lower than the previous estimates but it confirms the incompatibility of Hf and Zr in amphibole and clinopyroxene.

Zr and Hf contents in garnets in the studied granulites are in opposition to amphibole and clinopyroxene with $Hf_N \sim 0.5 \times Zr_N$. $D_{Zr}^{Grt/Cpx}$ as measured in the granulites from Central Finland is about 0.2 suggesting very low $D_{Zr}^{Grt/melt}$ in the range of 0.03–0.06 which is supported by the garnet/leucosome ratio in outcrop 36. These values strongly contrast with published $D_{Zr}^{Grt/melt}$ that are about one magnitude higher (Klein et al. 2000; van Westrenen et al. 2001; Barth et al. 2002), but agree with low $D_{Zr}^{Grt/Cpx}$ from other natural occurrences of mafic granulites (Storkey et al. 2005; Schröter et al. 2004; Schröter 2006) and garnet pyroxenites (Zack et al. 1997). Since $D_{Hf}^{Grt/Cpx} \sim 0.05-0.08$,, we also consider Hf partitioning into garnet from the mafic granulites as insignificant.

While Zr and Hf partitioning is very similar in amphibole and clinopyroxene, major differences are evident for Nb and Ta partitioning because they enter the M1-site in amphibole where they help to charge-balance dehydrogenation (Tiepolo et al. 2000). Amphiboles in the granulites are dehydrogenated, which allows increased incorporation of Nb and Ta, resulting in high $D_{Nb}^{Amph/Cpx}$ and $D_{Ta}^{Amph/Cpx}$. Niobium partition coefficients for amphibole in equilibrium with a tonalitic or andesitic melt generally range from 0.2 to 0.7 (Klein et al. 1997; Brenan et al. 1995; Hilyard et al. 2000; Xiong 2006). This is in accordance with the amphibole/leucosome ratio that gives $D_{Nb}^{Amph/melt} = 0.55$. Tiepolo et al. (2000) developed an equation that relates $D_{Nb/Ta}^{Amph/melt}$ to the total titanium content and the Mg# of the amphibole. Applying that equation to the average amphibole composition in the Finnish granulites (Mg# 0.58 ± 0.07, Ti_{tot} 0.22 ± 0.07 apfu) yields a mean $D_{Nb/Ta}^{Amph/melt}$ of 1.53 and furthermore $D_{Ta}^{Amph/melt} = 0.36$. However, the observed $D_{Ta}^{Amph/melt} \sim 0.59$ between amphiboles in sample 36M1 and leucosome 36L2 is slightly higher than the calculated partition coefficient.

The role of amphibole in controlling the Nb and Ta budget is limited because of the presence of ilmenite within the granulites. Nb and Ta strongly partition into ilmenite presumably due to coupled substitutions with Ti^{4+} and Fe^{2+} (Ewart and Griffin 1994). $D_{(Nb,Ta)}^{Ilm/melt}$ of 11 and 18 are obtained using the ratios of Nb and Ta contents in ilmenite and amphibole from samples 36M1 and 12M1, respectively. These values are clearly higher than $D_{(Nb,Ta)}^{Ilm/melt} \sim 2$ determined by Zack and Brumm (1998) and Klemme et al. (2006), but are lower than $D_{(Nb,Ta)}^{Ilm/melt} \sim 50 - 85$ for phenocryst–matrix relationships in rhyolitic systems (Stimac and Hickmott 1994; Ewart and Griffin 1994).

Partitioning of the Large Ion Lithophile Elements (LILE) into granulite mineral phases

Amphibole, plagioclase and apatite are the main hosts for Sr, Ba and Rb. Amphibole incorporates Ba and Rb on the large A-site where they substitute for K and Na, whereas Sr is restrained to the M4-site together with Ca and the REE. All LILE substitute for Ca in plagioclase. An overall increase in Sr and Ba contents in the plagioclases from our samples correlates with decreasing anorthite content of the plagioclases. Increasing Sr and Ba partitioning with decreasing X_{An} of plagioclase has been described by Blundy and Wood (1991), Bindeman et al. (1998), Foley et al. (2002) and Bédard (2006). Mafic granulites have X_{An} 0.5–0.7 while intermediate granulites have more albitic plagioclase with X_{An} 0.25–0.5. Corresponding $D_{Sr}^{Pl/melt} = 2.7 - 7.3$ and $D_{Ba}^{Pl/melt} = 0.2 - 1.2$ have been calculated using equations 19a and 18a from Bédard (2006) while the regressions in Blundy and Wood (1991) and Bindeman et al. (1998) yield higher $D_{Sr}^{Pl/melt} = 9-10$ at low $X_{An.}$

The calculated partition coefficients for Sr and Ba strongly contrast with the values obtained from the plagioclase/leucosome ratio. Plagioclase in sample 36M1 contains about 210 ppm and has X_{An} 0.6 yielding $D_{Sr}^{Pl/melt} = 3.5$ and furthermore an equilibrium melt Sr content of 60 ppm. Considering 345 ppm Sr in leucosome 36L2, the leucosome Sr content is clearly too high for the leucosome being representative for the melt phase in equilibrium with the plagioclase in sample 36M1. We observed that plagioclase in leucosome 36L2 has considerably lower X_{An} 0.35 compared to the supposed residue

36M1. This indicates that the leucosome crystallized from a melt phase enriched in Na as would be expected in equilibrium with Ca-rich plagioclase in 36M1 (Beard and Lofgren 1991). The misfit of the Sr and Ba data points to the limited usefulness of leucosomes as melt composition tracers, and to the probable enrichment of sodic plagioclase components in the leucosome due to crystallization of plagioclase in the former melt channelways.

Besides plagioclase, amphibole is a significant host for Ba in the granulites and also incorporates small amounts of Sr. $D_{Sr}^{Pl/Amph}$ between 9.2 and 15 were obtained from the analyses with the highest ratios measured in the granulite patches in diatexite, e.g. samples with the most sodic plagioclase. Hence, Sr is incompatible in amphibole and $D_{Sr}^{Amph/melt}$ falls in the range 0.3–0.6 which is in agreement with experimental as well as phenocryst–matrix data (Sisson 1994; Brenan et al. 1995). Measured $D_{Ba}^{Pl/Amph} \sim 1$ suggest $D_{Ba}^{Amph/melt}$ in the same range as $D_{Ba}^{Pl/melt}$.

Apatite contains about 1/3 as much Sr as plagioclase from the same sample. The plagioclase from the two samples in which apatite was analysed has X_{An} 0.35–0.4 and a corresponding $D_{Sr}^{Pl/melt} \sim 5.5$. $D_{Sr}^{Ap/melt}$ is therefore 1.7, similar to experimental data from Prowatke and Klemme (2006) for basaltic andesite and to data from Watson and Green (1981).

Transition metals

Sc, V, Cr and Ni are hosted by all mineral phases except for plagioclase and apatite. The relationships are complex but some simple conclusions can be drawn. The distribution of the transition metals among the principal minerals is consistent and applies for low concentrations in intermediate granulites as well as for high concentrations in mafic granulites, which stresses the near equilibrium conditions in the various granulite outcrops.

Partitioning of Ni into garnet is negligible. Orthopyroxene incorporates significantly lower amounts of Sc, Cr and V but similar amounts of Ni to the other minerals. Incorporation of Ni, Cr and V into amphibole is about 2 times higher than in clinopyroxene while Sc is equally distributed between the two minerals. Similar mineral/mineral ratios were reported from other occurrences of mafic granulites (Storkey et al. 2005; Schröter 2006). It is difficult to constrain partitioning in magnetite since the concentrations of V, Cr and Ni vary greatly within one sample. However, the LA-ICP-MS data indicate that concentrations of Ni, Cr and V are 3–10 times higher in magnetite than in clinopyroxene.

Up to now, there have been no well-constrained partition coefficient data sets for the transition metals. The spread in the published values is large and erratic and values for all four elements have not been reported together. Most existing data were derived from phenocryst–matrix compositions where bulk matrix effects are difficult to constrain, phenocrysts and matrix may be far from equilibrium, and the crystallization temperatures may be inappropriate for extrapolation to granulites.

Table 6 reports the overall $D^{mineral/Cpx}$ for the transition metals, the $D^{mineral/leucosome}$ as observed in outcrop 36 and calculated $D^{mineral/melt}$. $D^{mineral/leucosome}$ as given in Table 6 are considered to be a good approach to a consistent set of mineral/melt partition coefficients for the transition metals since they clearly reflect the overall observed concentration ratios in the granulite samples. Nevertheless, some of the values are in conflict with published data. For instance, $D^{Amph/melt}$ for the transition metals from Sisson (1994) agree with our data in having $D_{Sc}^{Amph/melt} \sim 2D_{Cr}^{Amph/melt}$, but their $D_{V}^{Amph/melt}$ are lower than $D_{Sc}^{Amph/melt}$ which is not observed in our data. Experimental partition coefficients from Dostal et al. (1983) yield $D_{Cr}^{Amph/melt} \sim 2 * D_{Ni}^{Amph/melt}$, as for our data, but their $D_{V}^{Amph/melt}$ are lower. The relatively high values for $D_{V}^{Amph/melt}$ for the Finnish granulites indicate more reducing conditions than in the volcanic rocks studied by Dostal et al. (1983) and Sisson (1994), as D_V for both oxide and silicate minerals increase with decreasing oxygen fugacity (Horn et al. 1994; Canil and Fedortchouk 2001).

The observation that $D_{Sc}^{Grt/melt}$ is larger than $D_{V}^{Grt/melt}$ and $D_{Cr}^{Grt/melt}$ is supported by findings of Hauri et al. (1994) and

Table 6 Range of $D^{mineral/Cpx}$, the mineral/leucosome ratio as observed in outcrop 36 and overall calculated $D^{mineral/melt}$ for the transition metals

	Overall $D^{mineral/Cpx}$				$D^{mineral/leucosome}$ as observed in outcrop 36				Overall $D^{mineral/melt}$ ($D^{Cpx/leucosome} \times D^{mineral/Cpx}$)			
	Sc	V	Cr	Ni	Sc	V	Cr	Ni	Sc	V	Cr	Ni
Cpx	–	–	–	–	11	7.3	2.5	1.7	–	–	–	–
Grt	0.8–1.5	0.4–0.6	1.2–2.3	0.02–0.05	15	2.6	2.5	0.06	9–16	3.0–4.4	3–6	0.03–0.08
Amph	0.7–1.1	1.3–2.4	1.0–3.7	1.5–2.5	12	12	6.1	3.2	8–12	9–17	3–9	2.5–4.2
Opx	0.13–0.24	0.16–0.23	0.16–0.42	1.0–1.2	–	–	–	–	1.4–2.6	1.2–1.7	0.4–1.0	1.7–2.0
Ilm	0.15–0.4	1.5–3.4	0.7–1.4	0.2–0.3	4.3	12	2.7	0.5	1.6–4.4	11–25	1.7–3.5	0.3–0.5

No $D^{Opx/leucosome}$ values are given because Opx does not belong to the peak metamorphic assemblage in sample 36M1

Sisson and Bacon (1992) although there is a large difference between the absolute values.

Our data confirm that the transition metals are compatible in amphibole, clinopyroxene, orthopyroxene, garnet, and ilmenite except for Ni in garnet. The values are lower than partition coefficients for high-silica melts (rhyolites, trachytes) but higher than most basaltic data.

Implications for melting within the lower crust

The modal abundances given in Table 1 and the mineral/melt partition coefficients constrained in this work were used for the calculation of bulk rock partition coefficients. This shows that, during anatexis of mafic and intermediate igneous rocks, Rb, Ba, Nb, Ta, Zr and Hf are strongly incompatible in the granulitic residue. The fractionation of Nb from Ta during the melting of mafic source rocks is a key factor in understanding the generation of Archean TTG-crust (Foley et al. 2002; Rapp et al. 2003; Pfänder et al. 2007). Distinctly lower Nb/Ta in Archean TTG compared to the bulk silicate earth ($\sim$14) and basaltic crust ($\sim$16) requires a mineral phase that preferentially incorporates Nb over Ta during partial melting of basaltic crust (Pfänder et al. 2007). Low-Mg amphibole has $D^{Nb/Ta} > 1$ (Tiepolo et al. 2000; Foley et al. 2002), whereas in Ti-phases (rutile, titanite, ilmenite) $D^{Nb/Ta} < 1$ must occur due to the Ti site being smaller than both Ta and Nb (Foley 2008). Therefore, low Nb/Ta can be expected in melts that are in equilibrium with a low-Mg amphibole-bearing residue but high Nb/Ta are inferred when the Nb/Ta ratio in melts is controlled by Ti-phases.

During amphibole-dehydration melting of mafic to intermediate amphibolitic source rocks within the lower crust the modal abundance of amphibole constantly decreases. Amphibole breakdown liberates significant amounts of Ti, which becomes available for the formation of Ti-phases such as ilmenite, should appropriate oxidation states prevail. Thus, the ratio of amphibole/ilmenite may become crucial in mafic granulites where amphibole is almost reacted out and ilmenite is present in modal abundances of up to 1 wt% (Table 3). A non-modal batch-melting model was applied to model Nb/Ta in melts as a function of amphibole and ilmenite abundance in the residue using Nb and Ta partition coefficients as constrained in this study. The melting model relies on the stoichiometry of weight proportion melting reactions given in Sen and Dunn (1994). We combined the quartz-present melting and quartz-absent melting reactions from Sen and Dunn (1994) so that quartz reacts out after about 10% melting. This requires 2.5% quartz in the source amphibolite. Additionally, we allowed an incremental increase of 0.05% ilmenite per 1% melting degree. An Archean amphibolite from central Finland served as the starting composition.

Two amphibolites were modelled, differing in their initial modes of amphibole, clinopyroxene and plagioclase prior to melting (Table 7). The amphibole-rich source rock yields up to 22% melt but the garnet contents in the residue are higher and plagioclase contents lower than in the mafic granulites. The observed modes of the mafic granulites (Table 3) are more consistent with low amounts of amphibole prior to melting so that the residue contains more plagioclase but less garnet.

According to our calculations, low Nb/Ta ratios of 12–13 as typical for the continental crust (Pfänder et al. 2007) are favoured by low degrees of melting and a high amount of residual amphibole (Fig. 10). In the case of a low initial abundance of amphibole, as suggested for the precursor rocks of the mafic granulites, amphibole would quickly become exhausted and Nb/Ta in the melt rises steeply so that the last batches of melt close to the elimination of amphibole will have elevated Nb/Ta. Ilmenite does not influence Nb/Ta in partial melts as strongly as would rutile in eclogite melting (Foley et al. 2002) because

Table 7 Input parameter and results of the non-modal batch melting model

Mineral assemblages	Amph	Qtz	Pl	Grt	Cpx	Ilm
Amphibole-rich source rock	**60**	**2.5**	**30**	**–**	**7.5**	**–**
Residue after 22% non-modal batch melting of the amphibole-rich source rock	<3	–	18	27	51	1.2
Amphibole-poor source rock	**33**	**2.5**	**39**	**–**	**25**	**–**
Residue after 13% non-modal batch melting of the amphibole-poor source rock	<1	–	35	13	50	0.7
Composition	**Nb**	**Ta**	**Zr**	**Sm**	**Nb/Ta**	**Zr/Sm**
Source rock	3.30	0.23	45.0	4.20	14.3	10.7
Residue after 22% melting	1.73	0.11	12.2	4.23	15.4	2.90
Melt after 22% melting	11.3	0.51	100	7.16	22.1	14.0
Residue after 13% melting	1.54	0.10	18.7	4.02	15.5	4.66
Melt after 13% melting	16.1	0.77	161	7.75	20.9	20.8

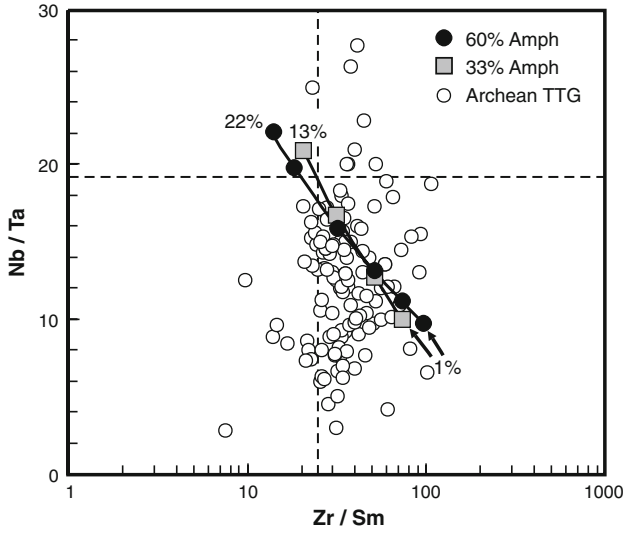

Fig. 10 Nb/Ta and Zr/Sm ratios in partial melts of mafic granulites as a function of degree of melting using a non-modal batch melting model and a combination of weight proportion melting reactions given in Sen and Dunn (1994). Incremental increase of ilmenite during progressive melting was allowed. Mineral/melt partition coefficients are taken from this study. Examples of Archean TTG (*white circles*) were compiled from the supplementary data of Condie (2005) and from the GeoRoc database (http://georoc.mpch-mainz.gwdg.de/georoc/). An Archean amphibolite from the working area with 3.30 ppm Nb, 0.23 ppm Ta, 45 ppm Zr and 4.20 ppm Sm served as the starting composition. *Black circles* show melts derived from an amphibolite consisting of 0.6 Amph, 0.3 Pl and 0.075 Cpx and 0.025 Qtz. In this case, Amph will become exhausted after 22% melting leaving a residue consisting of 0.05 Amph, 0.36 Pl, 0.12 Grt, 0.47 Cpx, 0.007 Ilm. *Grey squares* indicate melts derived from an amphibole-poor source rock consisting of 0.33 Amph, 0.39 Pl, 0.25 Cpx and 0.025 Qtz. After 13% melting the residue will be <0.01 Amph, 0.35 Pl, 0.13 Grt, 0.50 Cpx, 0.008 Ilm. The consumption of amphibole and the increase in ilmenite abundance lead to a steep increase of Nb/Ta in coexisting melts so that only very low degree melts fall into the TTG field. The strong decrease in Zr/Sm ratios is due to the smaller Sm partitioning into clinopyroxene compared to amphibole and consequently the liberation of Sm to the melt phase

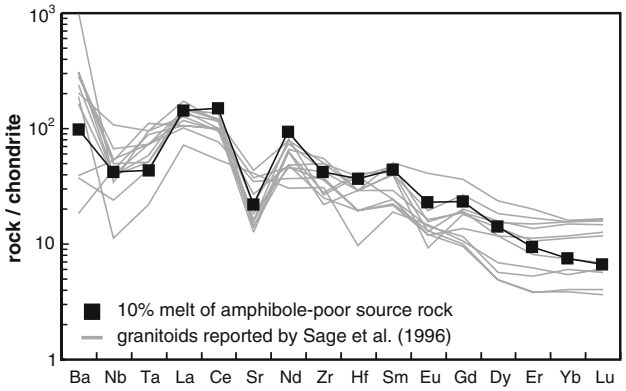

Fig. 11 Melt composition in equilibrium with granulitic residues after 10% melting of an amphibole-poor source rock modelled with the Qtz-present melting reaction from Sen and Dunn (1994) using the composition of an Archean amphibolite from the Iisalmi area and the partition coefficients constrained in this study. Model melts are similar to Archean granitoid rocks described by Sage et al. (1996). The spread in the HREE of the granitoids could be explained by more or less garnet involved in the melting reaction

of Nb and Ta partition coefficients in ilmenite being about a magnitude lower than in rutile.

Sr is compatible in the intermediate granulites because of the high modal abundance of plagioclase and its low anorthite component. Melts in equilibrium with the plagioclase-rich granulites will therefore be depleted in Sr. The partition coefficient for Sr becomes lower in the more Ca-rich mafic granulites but Sr remains compatible ($D_{Sr} > 1$) except for mafic granulites with the most anorthitic plagioclase and the lowest plagioclase contents. The retention of Sr in granulites due to high modal abundances of plagioclase precludes granulites, particularly intermediate ones, from being volumetrically important source rocks for TTG crust since high Sr contents are a key attribute of TTG (Martin and Moyen 2002). However, some rare Finnish samples (e.g. outcrop 036) indicate that melts with elevated Sr contents and more strongly fractionated REE-pattern are present, but they can only be derived from batches of granulite with the lowest plagioclase contents.

Although melts in equilibrium with granulitic residues may be volumetrically insignificant in Archean TTG genesis, they may nevertheless occur. Sage et al. (1996) reported on granitoid rocks from the Superior Province, Canada and attributed the geochemical features of these rocks to significant contamination of mantle melts by ancient sialic crust. However, small amounts of melting of amphibolites leaving plagioclase-rich granulites as residues can also explain the geochemical characteristics as well as the smallscale occurrence of these rocks (Fig. 11).

Within mafic granulites, the presence of garnet dictates the bulk compatibility of the HREE. Due to high $D_{HREE}^{grt/melt}$ mafic granulites would coexist with a strongly fractionated, HREE-depleted partial melt. However, garnet may have grown late during peak metamorphism and failed to equilibrate with the bulk matrix. Thus, presence of garnet has less influenced the composition of corresponding melts than may be expected at first sight from the modal abundance of garnet. Trace element analyses of minerals are therefore crucial to demonstrate equilibrium conditions and draw conclusions on melt compositions.

Conclusions

In situ trace element analyses of minerals from mafic and intermediate granulites were used to monitor partial

melting processes within the middle to lower crust. The LA-ICP-MS analyses report equilibrium partitioning between peak metamorphic phases except for minerals that grew together with garnet in small microdomains. We constrained a self-consistent set of $D^{\text{mineral/mineral}}$ and $D^{\text{mineral/melt}}$ values, using predictive models, experimental data and rarely occurring leucosomes with preserved melt composition. Constant mineral/mineral partition coefficients for the REE, HFSE and the transition metals among the principal minerals within compositionally diverse granulites imply that the ratios given here can be easily adopted for other granulite occurrences, giving a clear impression of trace element distribution in the lower crust.

LA-ICPMS analyses of large garnet porphyroblasts within mafic granulites indicate a lack of equilibrium between the porphyroblasts and the matrix regarding the REE. The detection of such small-scale disequilibrium features within an otherwise well-equilibrated granulite facies mineral assemblage strongly stresses the importance of in situ trace element analyses for understanding the development of metamorphic mineral assemblages and their trace element signature.

During metamorphism and partial melting certain trace elements are controlled by accessory phases, which are highlighted by analyses of apatite and ilmenite. Because of the strong affinity of ilmenite towards Nb and Ta its role may become crucial as the amount of amphibole progressively diminishes during dehydration melting so that ilmenite becomes the major host for Nb and Ta and consequently controls Nb/Ta ratios in coexisting melts.

$D^{\text{mineral/melt}}$ defined in this study are applicable for low pressure, high temperature partial melting reactions and intermediate to silicic melt compositions. Non-modal melting models using these $D^{\text{mineral/melt}}$ showed that partial melts of amphibolites leaving mafic and intermediate granulites as residues at melting degrees <15% will be different from typical Archean TTG-crust mainly because of negative Sr-anomalies due to high amounts of plagioclase in the residues. Still, the models demonstrate what kind of melts can be expected from crustal melting of amphibolitic source rocks and help to distinguish them from magmatic rocks derived under plagioclase-absent conditions.

Acknowledgments The support of Dorrit Jacob and Matthias Barth during the LA-ICP-MS analyses is greatly appreciated. The Geological Survey of Finland supported fieldwork in central Finland. This work was supported by the German Research Foundation (Graduate School "Composition and Evolution of Crust and Mantle") and the Geocycles Cluster of the State of Rhineland-Palantine. This is Geocycles Publication No. 621.

Appendix 1

See Table 8.

Table 8 Representative EMP analyses of major mineral phases

Sample	Type	Phase	SiO_2	TiO_2	Al_2O_3	FeO	MnO	MgO	CaO	Na_2O	K_2O	Total
02M2	Grt–Cpx granulite	Cpx	50.0	0.46	3.53	12.3	0.21	10.9	22.2	0.48	–	100.3
		Grt	38.4	0.08	21.3	26.3	1.61	3.86	9.96	0.02	0.01	101.8
		Pl	53.5	–	29.2	0.20	0.01	0.01	12.0	4.96	0.10	100.0
34M2	Grt–Cpx granulite	Cpx	50.2	0.34	3.02	11.2	0.26	11.9	22.0	0.41	–	99.6
		Grt	38.5	0.09	21.4	25.5	1.09	6.03	8.00	–	–	100.7
		Pl	54.5	–	29.6	0.05	–	0.01	11.4	5.00	0.05	100.7
36M1	Grt–Cpx granulite	Amph	44.1	1.76	11.1	14.9	0.14	12.6	11.3	2.06	0.37	98.6
		Cpx	51.9	0.29	3.04	10.1	0.23	13.2	22.3	0.42	–	101.6
		Grt	39.3	0.07	21.8	25.5	0.83	7.29	6.84	0.01	–	101.8
		Pl	53.7	–	29.8	0.10	0.02	0.02	12.7	4.70	0.03	101.0
		Il	0.79	50.1	0.20	46.4	0.58	1.19	0.02	0.04	0.02	99.6
		Mgt	0.34	0.67	0.59	90.6	0.04	0.15	0.02	0.01	–	94.5
140M	Grt–Cpx granulite	Cpx	51.3	0.37	2.98	11.3	0.19	11.9	22.2	0.45	0.01	100.8
		Grt	37.3	0.09	21.1	26.0	1.08	4.97	8.27	–	–	99.0
		Pl	51.0	–	31.7	0.10	–	0.01	13.9	3.59	0.02	100.3
		Il	0.03	52.8	0.01	45.8	0.80	0.37	0.01	0.01	–	100.0

Table 8 continued

Sample	Type	Phase	SiO_2	TiO_2	Al_2O_3	FeO	MnO	MgO	CaO	Na_2O	K_2O	Total
12M1	Grt–Cpx granulite	Amph	43.9	2.09	11.5	13.8	0.23	12.9	11.7	1.57	0.98	99.2
		Cpx	51.1	0.32	3.56	10.6	0.34	12.7	21.8	0.60	0.01	101.0
		Grt	39.2	0.12	21.7	25.4	1.34	7.92	6.41	0.01	0.01	102.1
		Pl	57.7	0.01	26.5	0.06	0.02	–	8.78	6.87	0.10	100.2
		Il	0.03	50.4	0.02	47.4	1.18	0.67	0.01	0.01	–	99.8
		Mgt	0.08	0.12	0.28	92.6	0.02	0.06	–	0.03	–	93.9
49M	Grt–Cpx granulite	Amph	41.3	3.07	12.0	19.8	0.13	8.77	11.3	1.73	1.66	100.2
		Cpx	51.0	0.28	2.72	14.7	0.24	11.3	20.4	0.61	–	101.3
		Grt	38.4	0.08	21.3	29.6	1.28	4.71	6.59	0.01	–	102.1
		Opx	50.9	0.05	0.86	32.9	0.64	16.1	0.76	0.01	–	102.2
		Pl	60.0	0.01	25.3	0.04	0.03	0.01	7.22	7.71	0.34	100.6
76M1	Grt–Cpx granulite	Amph	41.6	3.24	11.8	19.7	0.13	8.54	11.3	1.83	1.62	100.0
		Cpx	51.0	0.23	2.48	13.5	0.27	10.9	21.7	0.64	0.01	100.7
		Grt	38.4	0.04	21.1	29.6	1.46	4.23	7.11	0.01	0.01	101.9
		Pl	59.5	0.01	24.8	0.07	0.01	0.01	7.18	7.62	0.35	99.6
76a	Opx-Cpx granulite	Amph	44.1	1.79	10.9	14.2	0.16	12.4	11.4	1.58	0.70	97.4
		Cpx	51.8	0.25	2.76	9.54	0.29	13.3	21.9	0.55	–	100.4
		Opx	52.3	0.06	1.57	24.5	0.61	21.5	0.51	0.03	0.01	101.1
		Pl	54.6	0.01	27.8	0.10	0.02	0.01	10.8	5.34	0.18	99.0
112M	Opx-Cpx granulite	Amph	44.6	1.55	10.8	13.8	0.16	12.7	11.3	1.49	0.74	97.2
		Cpx	50.8	0.21	2.79	9.39	0.28	13.0	22.2	0.52	0.02	99.4
		Opx	52.3	0.06	1.57	24.3	0.65	21.4	0.58	0.03	0.01	101
		Pl	54.8		28.0	0.07		0.01	9.56	6.06	0.19	98.8
80M	Opx-Cpx granulite	Amph	42.2	2.20	11.7	15.7	0.15	10.8	11.4	1.54	1.68	97.9
		Bt	36.6	4.90	14.4	17.1	0.06	12.6	–	0.08	9.72	96.5
		Cpx	51.5	0.17	2.24	11.3	0.28	12.6	21.0	0.65	–	99.8
		Opx	51.3	0.06	1.15	27.9	0.61	19.0	0.52	0.01	0.01	100.6
		Pl	58.9	–	25.0	0.08	0.03	0.01	6.67	7.59	0.49	98.8
102a	Opx-Cpx granulite	Amph	42.7	2.12	11.1	16.4	0.31	10.6	11.4	1.44	1.51	97.6
		Cpx	52.1	0.16	2.30	11.0	0.51	12.4	21.5	0.83	–	100.8
		Opx	51.8	0.06	1.36	26.7	1.12	18.4	0.60	0.02	0.02	100.1
		Pl	61.5		24.8	0.03		0.01	5.75	8.36	0.23	100.7
114M	Opx-Cpx granulite	Amph	42.8	2.05	11.1	15.2	0.26	11.8	11.4	1.62	1.58	97.7
		Cpx	52.3	0.18	2.25	11.9	0.51	13.6	19.5	0.77	0.01	101.1
		Opx	52.3	0.04	1.06	24.6	1.04	21.3	0.51	0.03	0.01	100.9
		Pl	61.1		25.0	0.12		0.01	6.13	8.26	0.25	100.9

Appendix 2

See Table 9.

Table 9 LA-ICP-MS analyses of mineral phases

Sample	Mineral	Sc	V	Cr	Ni	Rb	Sr	Y	Zr	Nb	Ba	La	Ce
002M2	Cpx	81.1	558	395	178	0.046	7.77	4.80	53.9	0.031	0.199	1.78	9.19
Grt–Cpx granulite	Grt	72.2	264	917	3.87	–	0.177	124	7.17	0.004	0.251	0.162	0.503
	Pl	1.35	0.423	3.02	1.22	0.094	287	0.051	0.055	–	56.2	1.93	3.16
034M2	Cpx 1	81.6	n.a.	440	176	0.135	5.99	7.86	57.3	0.059	0.371	1.56	10.8
Grt–Cpx granulite	Cpx 2	90.2	n.a.	452	159	0.085	4.55	32.7	51.9	0.072	0.776	0.999	8.55
	Grt 1	101	242	554	5.00	–	0.040	77.2	12.0	0.010	0.018	0.008	0.087
	Grt 2	100	255	539	4.82	–	0.035	99.2	11.0	0.011	0.033	0.095	0.196
	Pl	n.a.	n.a.	n.a.	n.a.	0.777	236	n.a.	n.a.	n.a.	25.9	1.55	3.56
036M1	Amph 1	91.2	974	474	146	1.07	25.6	27.0	51.7	3.92	11.3	2.40	11.3
Grt–Cpx granulite	Amph 2	93.6	985	441	125	1.41	20.8	41.8	49.5	3.75	11.2	2.35	11.9
	Amph 3	111	1075	508	126	1.39	18.3	66.8	44.4	3.95	9.57	2.60	13.9
	Cpx 1	82.9	547	128	64.4	0.053	6.27	6.92	47.0	0.020	0.084	0.822	4.57
	Cpx 2	94.6	587	236	78.2	0.087	4.99	19.1	50.9	0.038	0.646	0.803	4.16
	Cpx 3	93.8	540	217	61.7	0.040	3.05	45.3	48.5	0.092	0.282	0.772	4.30
	Grt	117	217	197	2.48	–	0.079	101	9.54	0.015	0.054	0.064	0.154
	Pl	1.36	0.215	3.11	5.44	0.081	216	0.313	–	–	10.8	1.09	1.87
	Ilm	34.6	977	212	20.6	–	–	0.107	8.80	82.1	–	0.320	0.197
	Mgt	2.45	2476	990	320	–	–	1.41	0.313	0.576	–	0.091	0.228
140M	Cpx	64.0	407	516	215	–	6.76	4.51	47.1	0.018	0.717	1.22	5.60
Grt–Cpx granulite	Grt	69.2	238	711	4.13	–	0.603	149	9.54	0.028	0.307	0.031	0.047
	Pl	6.71	2.95	7.72	2.83	0.021	283	0.036	0.307	–	20.1	1.61	2.32
	Ilm	9.39	611	715	66.5	–	–	0.276	2.50	124	–	–	0.186
012M1	Amph	85.9	374	60.7	104	1.18	58.1	127	47.5	9.12	270	27.6	105
Grt–Cpx granulite	Cpx1	103	285	55.4	56.7	0.036	18.8	57.0	59.0	0.077	1.62	8.72	39.7
	Cpx2	70.6	297	46.4	64.0		18.9	14.7	87.5			10.2	38.3
	Grt	106	122	64.0	2.03	0.213	–	205	18.2	0.065	–	0.076	0.331
	Ilm	44.4	1032	70.4	19.6	–	–	0.360	22.6	396	–	1.89	1.83
	Mgt	0.340	2026	630	88.3	–	–	0.070	0.026	1.39	–	0.223	0.282
	Pl	n.a.	n.a.	n.a.	n.a.	0.070	700	n.a.	n.a.	n.a.	288	8.35	11.2
	Ap 1	–	8.76	–	3.31	–	214	389	–	0.048	1.05	834	1844
	Ap 2	–	12.8	–	0.670	–	232	361	0.593	0.174	0.550	232	828
	Ap 3	–	6.45	–	3.52	–	209	329	0.459	–	4.38	44.2	245
049M	Amph 1	131	1101	380	111	3.49	73.9	80.7	40.5	8.85	264	17.3	52.5
Grt–Cpx granulite	Amph 2	127	885	331	106	3.17	68.2	94.2	44.1	8.49	265	16.9	50.2
	Cpx 1	102	n.a.	111	65.8	0.136	16.2	12.3	69.7	0.015	0.112	4.87	18.3
	Cpx 2	131	705	255	60.9	0.073	16.1	24.2	49.9	0.041	0.770	5.03	18.5
	Cpx 3	122	n.a.	161	64.7	0.152	14.9	31.0	46.1	0.024	0.453	4.16	13.9
	Grt	82.1	282	211	1.38	–	0.062	206	13.9	0.020	–	0.106	0.311
	Opx	27.7	150	64.5	68.7	0.118	0.378	2.86	0.933	0.006	0.308	0.094	0.178
	Pl	4.96	0.185	–	4.53	0.155	643	0.069	0.045	–	301	3.71	4.45
	Ap 1	–	4.83	–	12.7	0.155	300	156	24.4	113	0.004	330	716
	Ap 2	–	7.24	–	15.0	0.558	191	288	1.28	47.7	–	480	993
	Ap 3	–	3.54	–	2.29	0.265	185	339	0.495	0.523	0.014	418	795
076M1	Amph	72.0	521	2.42	16.0	2.69	77.3	19.9	38.6	12.4	290	37.7	99.0
Grt–Cpx granulite	Cpx	85.0	263	2.18	9.90	0.253	19.4	6.66	40.9	0.131	3.56	8.57	26.6
	Grt	78.8	175	3.21	0.569	0.060	0.193	140	6.90	0.033	0.086	0.082	0.282
	Pl	n.a.	n.a.	n.a.	n.a.	0.200	724	n.a.	n.a.	n.a.	238	7.78	7.08

Table 9 continued

Sample	Mineral	Sc	V	Cr	Ni	Rb	Sr	Y	Zr	Nb	Ba	La	Ce
076a	Amph	80.2	444	92.3	101	2.14	45.2	33.7	33.4	5.65	60.3	9.85	32.0
Opx-Cpx granulite	Cpx	84.6	221	16.8	43.2	–	13.5	10.0	33.9	0.063	0.851	2.99	10.6
	Opx	15.8	65.9	205	52.9	0.097	0.754	0.347	0.670	n.a.	0.224	0.023	0.046
	Pl	n.a.	n.a.	n.a.	n.a.	0.088	542	n.a.	n.a.	n.a.	93.3	4.36	5.25
112M	Amph	86.4	474	21.7	101	0.874	41.5	33.5	40.9	5.98	72.5	11.4	33.4
Opx-Cpx granulite	Cpx	80.0	201	6.93	41.3	0.070	21.9	9.57	35.3	0.050	3.83	3.39	10.4
	Opx	n.a.	n.a.	n.a.	n.a.	0.027	0.305	n.a.	n.a.	n.a.	0.299	0.020	0.036
	Pl	n.a.	n.a.	n.a.	n.a.	0.418	510	n.a.	n.a.	n.a.	134	4.16	4.29
080M	Amph	73.2	552	1485	372	5.38	33.5	136	34.8	32.1	123	46.3	168
Opx-Cpx granulite	Cpx	76.2	n.a.	436	199	0.118	11.7	50.3	33.8	0.071	0.963	11.3	46.7
	Opx	12.8	n.a.	157	208	0.307	0.725	2.72	0.625	0.014	1.72	0.405	0.434
	Pl	n.a.	n.a.	n.a.	n.a.	0.394	458	n.a.	n.a.	n.a.	117	11.8	14.6
102a	Amph	142	180	334	109	5.34	42.7	237	60.21	36.4	107	69.7	233
Opx-Cpx granulite	Cpx	203	107	214	63.6	0.084	15.9	85.0	47.11	0.110	0.410	13.2	55.6
	Opx	32.8	19.5	35.0	66.3	0.091	0.753	3.58	0.471	0.051	0.272	0.367	0.906
	Pl	1.16	0.263	3.46	0.685	0.303	636	0.178	–	0.019	127	15.1	17.9
114M	Amph	78.7	466	15.2	77.0	9.53	44.1	53.1	62.54	13.8	64.9	20.7	67.9
Opx-Cpx granulite	Cpx	107	280	12.4	48.3	0.227	14.7	19.2	50.60	0.082	0.443	4.88	18.9
	Opx	14.1	43.6	5.21	52.5	0.030	0.446	0.634	0.855	–	0.229	0.075	0.183
	Pl	2.78	5.67	4.01	1.58	0.275	643	0.255	0.40	0.032	65.8	5.73	6.71

Sample	Mineral	Nd	Sm	Eu	Gd	Dy	Er	Yb	Lu	Hf	Ta	Th	U
002M2	Cpx	11.1	3.40	0.680	2.93	1.53	0.371	0.215	0.027	2.30	0.012	0.008	0.004
Grt–Cpx granulite	Grt	1.55	2.56	1.14	8.70	19.0	15.1	17.4	2.68	0.101	0.002	0.004	0.003
	Pl	0.848	0.083	0.645	0.048	0.020	0.011	–	0.020	0.045	–	0.015	0.028
034M2	Cpx 1	17.5	6.04	1.22	5.33	2.51	0.587	0.324	0.032	2.87	0.009	0.005	0.004
Grt–Cpx granulite	Cpx 2	17.8	7.26	1.29	8.81	7.82	3.00	1.93	0.234	2.78	0.007	0.004	0.003
	Grt 1	1.36	2.57	1.26	8.58	15.6	6.52	3.95	0.395	0.162	0.001	0.001	0.001
	Grt 2	1.30	2.59	1.28	8.18	17.3	10.7	6.97	0.769	0.130	0.003	0.004	0.011
	Pl	1.32	0.144	0.900	0.070	0.021	–	–	–	n.a.	n.a.	n.a.	n.a.
036M1	Amph 1	16.7	7.50	1.91	8.32	7.36	2.51	1.03	0.120	2.36	0.148	0.049	0.012
Grt–Cpx granulite	Amph 2	18.3	7.55	2.10	11.4	9.66	3.94	3.33	0.482	2.55	0.136	0.036	–
	Amph 3	22.3	9.56	2.49	13.1	14.3	6.63	4.89	0.778	2.46	0.166	–	0.011
	Cpx 1	6.70	2.74	0.780	3.22	2.26	0.591	0.248	0.026	1.99	0.006	0.013	0.010
	Cpx 2	6.77	2.92	0.695	3.91	4.00	1.94	1.79	0.257	2.38	0.005	0.018	0.010
	Cpx 3	7.25	3.40	0.821	5.45	8.11	5.09	4.98	0.698	2.43	0.007	0.018	0.010
	Grt	0.521	1.33	0.733	5.85	15.4	12.8	15.4	2.35	0.145	0.002	0.014	0.019
	Pl	0.625	0.093	0.499	0.082	0.052	0.025	–	–	0.050	–	0.030	–
	Ilm	0.116	–	0.349	–	–	–	0.034	0.014	0.543	4.35	0.005	0.011
	Mgt	0.258	0.359	0.054	0.570	0.390	0.238	0.392	0.032	0.045	0.043	0.004	0.005
140M	Cpx	8.08	2.81	0.553	3.03	1.83	0.382	0.144	0.018	1.88	0.010	0.061	0.021
Grt–Cpx granulite	Grt	0.651	1.54	0.729	6.86	20.3	19.7	23.7	4.10	0.136	–	0.012	0.012
	Pl	0.558	0.071	0.496	0.042	0.018	–	0.018	–	0.046	0.020	–	–
	Ilm	–	0.059	–	–	–	0.043	0.094	0.035	0.086	8.69	0.009	0.036

Table 9 continued

Sample	Mineral	Nd	Sm	Eu	Gd	Dy	Er	Yb	Lu	Hf	Ta	Th	U
012M1	Amph	109	29.3	7.80	30.1	27.2	12.3	10.1	1.52	2.56	0.289	0.059	0.024
Grt–Cpx granulite	Cpx1	42.6	12.5	3.02	12.8	12.7	6.59	5.82	0.824	2.81	0.012	0.039	0.008
	Cpx2	42.5	12.0	2.95	10.0	5.26	1.16	0.548	0.103	3.03		0.116	70.6
	Grt	3.24	4.82	2.63	15.9	32.0	22.6	23.4	3.74	0.257	–	–	0.118
	Ilm	0.517	0.187	0.048	0.087	0.057	0.251	0.402	0.092	1.49	18.9	0.550	0.037
	Mgt	0.187	0.300	0.025	0.110	0.049	0.044	0.067	–	0.027	0.097	–	0.001
	Pl	2.44	0.211	1.41	0.102	0.044	0.017	0.014	0.037	n.a.	n.a.	n.a.	n.a.
	Ap 1	979	185	31.4	148	84.9	32.0	19.4	2.45	–	–	4.28	2.21
	Ap 2	624	128	23.4	118	71.9	34.1	19.7	2.97	–	–	5.29	2.38
	Ap 3	326	89.5	20.4	96.6	67.1	31.1	19.8	2.72	–	–	2.71	1.85
049M	Amph 1	47.1	14.3	3.10	17.3	16.2	8.38	6.74	0.808	2.83	0.367	0.160	0.035
Grt–Cpx granulite	Amph 2	43.1	12.7	2.96	15.9	17.4	10.1	9.48	1.35	2.82	0.431	0.176	0.038
	Cpx 1	19.7	6.53	1.32	6.52	3.85	0.922	0.517	0.052	3.81	0.007	0.067	0.010
	Cpx 2	18.7	5.94	1.15	6.68	5.99	2.47	1.90	0.270	3.41	0.007	0.079	0.016
	Cpx 3	12.6	4.11	0.914	5.13	6.05	3.63	3.76	0.573	2.86	0.007	0.074	0.015
	Grt	1.52	3.10	1.27	12.2	28.9	23.9	28.2	4.46	0.198	0.006	0.022	0.005
	Opx	0.153	0.089	0.025	0.205	0.490	0.545	0.998	0.191	0.068	0.001	0.043	0.001
	Pl	0.771	0.069	0.976	0.050	0.019	0.008	–	0.002	–	–	–	–
	Ap 1	403	83.5	10.2	77.4	39.1	12.1	5.77	0.755	1.12	0.023	4.85	2.74
	Ap 2	527	102	9.72	100	61.3	25.8	13.9	1.98	–	–	7.39	4.22
	Ap 3	372	76.3	9.40	77.9	60.6	32.4	22.7	3.17	–	0.007	7.17	4.09
076M1	Amph	57.1	11.2	2.48	9.24	5.68	1.64	0.913	0.110	2.55	0.600	0.187	0.030
Grt–Cpx granulite	Cpx	16.9	3.53	0.761	3.00	1.92	0.573	0.355	0.053	2.37	0.016	0.046	0.019
	Grt	1.65	2.51	1.10	8.48	20.2	17.0	19.4	3.16	0.142	0.001	–	0.002
	Pl	0.856	0.084	0.599	0.115	–	–	–	0.013	n.a.	n.a.	n.a.	n.a.
076a	Amph	22.9	5.44	1.44	5.80	6.18	3.62	3.54	0.509	n.a.	0.247	0.106	0.037
Opx-Cpx granulite	Cpx	7.52	1.71	0.499	1.83	2.08	1.08	1.12	0.184	n.a.	0.015	0.025	0.012
	Opx	0.041	–	0.010	0.050	0.074	0.094	0.223	0.050	n.a.	n.a.	n.a.	n.a.
	Pl	0.749	0.062	0.299	0.032	0.025	0.016	–	–	n.a.	n.a.	n.a.	n.a.
112M	Amph	22.3	5.04	1.35	5.64	6.05	3.55	3.40	0.534	n.a.	0.322	0.143	0.068
Opx-Cpx granulite	Cpx	6.90	1.61	0.416	1.64	1.83	1.08	1.06	0.160	n.a.	–	0.037	0.007
	Opx	0.035	–	0.011	0.053	0.066	0.099	0.224	0.045	n.a.	n.a.	n.a.	n.a.
	Pl	0.623	0.177	0.288	0.064	–	–	–	–	n.a.	n.a.	n.a.	n.a.
080M	Amph	121	27.2	3.03	26.7	23.6	13.8	12.9	1.73	n.a.	1.78	0.724	0.069
Opx-Cpx granulite	Cpx	37.6	9.29	0.968	9.11	9.31	5.42	5.53	0.808	2.51	0.025	0.133	0.023
	Opx	0.296	0.083	0.016	0.147	0.304	0.403	0.844	0.163	0.059	0.003	0.194	0.030
	Pl	2.26	0.154	0.787	0.074	0.025	0.010	–	–	–	–	–	-
102a	Amph	197	49.9	4.26	48.1	45.8	24.3	20.6	2.85	3.59	1.43	0.333	0.044
Opx-Cpx granulite	Cpx	51.4	15.4	1.45	15.8	16.5	9.40	8.91	1.36	2.97	0.022	0.052	0.360
	Opx	0.469	0.148	0.020	0.194	0.470	0.596	1.45	0.270	0.068	–	–	–
	Pl	2.75	0.203	0.800	0.096	0.032	0.023	–	–	–	–	0.046	–
114M	Amph	51.1	10.7	2.39	10.1	9.51	5.53	5.72	0.872	2.85	1.26	0.682	0.368
Opx-Cpx granulite	Cpx	14.9	3.29	0.725	3.22	3.50	1.99	2.46	0.432	2.36	0.041	0.183	0.143
	Opx	0.123	0.076	0.019	0.088	0.136	0.193	0.503	0.113	0.080	0.019	0.105	0.218
	Pl	0.905	0.053	0.441	0.087	0.043	0.030	0.041	0.010	0.101	0.053	0.020	–

Minerals numbered 1–3 show the variation in the REE content within one sample

References

Armstrong JT (1995) CITZAF: a package of correction programs for the quantitative electron microbeam X-ray analysis of thick polished materials, thin films, and particles. Microbeam Anal 4:177–200

Bacon CR, Druitt TH (1988) Compositional evolution of the zoned calcalkaline magma chamber of Mount-Mazama, Crater Lake, Oregon. Contrib Mineral Petrol 98(2):224–256

Barth MG, Foley SF, Horn I (2002) Partial melting in Archean subduction zones: constraints from experimentally determined trace element partition coefficients between eclogitic minerals and tonalitic melts under upper mantle condiditons. Precamb Res 113:323–340

Bea F, Pereira MD, Stroh A (1994) Mineral/leucosome trace-element partitioning in a peraluminous migmatite (a laser ablation-ICP-MS study). Chem Geol 117:291–312

Beard JS, Lofgren GE (1991) Dehydration melting and water-saturated melting of basaltic and andesitic greenstones and amphibolites at 1, 3 and 6–9 kb. J Petrol 32:365–401

Bédard JH (2006) Trace element partitioning in plagioclase feldspar. Geochim Cosmochim Acta 70:3717–3742

Bindeman IN, Davis AM (2000) Trace element partitioning between plagioclase and melt: investigation of dopant influence on partition behaviour. Geochim Cosmochim Acta 64(16):2863–2878

Bindeman IN, Davies AM, Drake MJ (1998) Ion microprobe study of plagioclase-basalt experiments at natural concentration levels of trace elements. Geochim Cosmochim Acta 62(7):1175–1193

Blundy J, Wood B (1991) Crystal-chemical controls on the partitioning of Sr and Ba between plagioclase feldspar, silicate melts and hydrothermal solutions. Geochim Cosmochim Acta 55:193–209

Blundy J, Wood B (1994) Prediction of crystal-melt partition-coefficients from elastic-moduli. Nature 372(6505):452–454

Bottazzi P, Tiepolo M, Vannucci R, Zanetti A, Brumm R, Foley SF, Oberti R (1999) Distinct site preferences for heavy and light REE in amphibole and the prediction of D-Amph/L(REE). Contrib Mineral Petrol 137(1–2):36–45

Brenan JM, Shaw HF, Ryerson FJ, Phinney DL (1995) Experimental determination of trace element partitioning between pargasite and a synthetic hydrous andesitic melt. Earth Planet Sci Lett 135:1–11

Brice JC (1975) Some thermodynamic aspects of the growth of strained crystals. J Cryst Growth 28:249–253

Brown M (1994) The generation, segregation, ascent and emplacement of granite magma: the migmatite-to-crustally-derived granite connection in thickened orogens. Earth-Sci Rev 36:83–130

Canil D, Fedortchouk Y (2001) Olivine-liquid partitioning of vanadium and other trace elements, with applications to modern and ancient picrites. Can Mineral 39:319–330

Cawthorn RG (1996) Models for incompatible trace-element abundances in cumulus minerals and their application to plagioclase and pyroxenes in the Bushveld Complex. Contrib Mineral Petrol 123(1):109–115

Cawthorn RG, Collerson KD (1974) The recalculation of pyroxene end-member parameters and the estimation of ferrous and ferric iron content from electron microprobe analyses. Am Mineral 59:1203–1208

Chazot G, Menzies MA, Harte B (1996) Determination of partition coefficients between apatite, clinopyroxene, amphibole, and melt in natural spinel lherzolites from Yemen: implications for wet melting of the lithospheric mantle. Geochim Cosmochim Acta 60(3):423–437

Clarke GL, White RW, Lui S, Fitzherbert JA, Pearson NJ (2007) Contrasting behaviour of rare earth and major elements during partial melting in granulite facies migmatites, Wuluma Hills, Arunta Block, central Australia. J Metamorph Geol 25(1):1–18

Colson RO, McKay GA, Taylor LA (1988) Temperature and composition dependencies of trace-element partitioning—olivine melt and low-Ca pyroxene melt. Geochim Cosmochim Acta 52(2):539–553

Condie KC (2005) TTGs and adakites: are they both slab melts? Lithos 80:33–44

Dalpé C, Baker DR (2000) Experimental investigation of large-ion-lithophile-element-, high-field-strength-element- and rare-earth-element- partitioning between calcic amphibole and basaltic melt: the effects of pressure and oxygen fugacity. Contrib Mineral Petrol 140(2):233–250

Dostal J, Dupuy C, Carron JP, Guen Le, de Kerneizon M, Maury RC (1983) Partition coefficients of trace elements: application to volcanic rocks of St. Vincent, West Indies. Geochim Cosmochim Acta 47:525–533

Dunn T, Sen C (1994) Mineral/matrix partition coefficients for orthopyroxene, plagioclase and olivine in basaltic to andesitic systems: a combined analytical and experimental study. Geochim Cosmochim Acta 58(2):717–733

Ewart A, Griffin WL (1994) Application of proton-microprobe data to trace element partitioning in volcanic rocks. Chem Geol 117:251–284

Fedorowich JS, Richards JP, Jain JC, Kerrich R, Fan J (1993) A rapid method for REE and trace-element analysis using laser sampling ICP-MS on direct fusion whole-rock glasses. Chem Geol 106:229–249

Foley SF (2008) A trace element perspective on Archean crust formation and on the presence or absence of Archean subduction. Geol Soc Am Spec Publ 440:31–50

Foley SF, Tiepolo M, Vannucci R (2002) Growth of early continental crust controlled by melting of amphibolite in subduction zones. Nature 417:837–840

Fujimaki H (1986) Partition-Coefficients of Hf, Zr, and Ree between zircon, apatite, and liquid. Contrib Mineral Petrol 94(1):42–45

Garrido CJ, Bodinier J-L, Burg J-P, Zeilinger G, Hussain SS, Dawood H, Chaudhry S, Gervilla F (2006) Petrogenesis of mafic garnet granulite in the lower crust of the Kohistan Paleo-arc Complex (Northern Pakistan): implications for intra-crustal differentiation of island arcs and generation of continental crust. J Petrol 47(10):1873–1914

Glaser SM, Foley SF, Günther D (1999) Trace element compositions of minerals in garnet and spinel peridotite xenoliths from the Vitim volcanic field, Transbaikalia, eastern Siberia. Lithos 48:263–285

Green TH, Pearson NJ (1985) Rare earth element partitioning between clinopyroxene and silicate liquid at moderate to high pressure. Contrib Mineral Petrol 91:24–36

Hansen EC, Janardhan AS, Newton RC, Prame WKBN, Ravindra Kumar GR (1987) Arrested charnockite formation in southern India and Sri Lanka. Contrib Mineral Petrol 96:225–244

Harley SL (1989) The origins of granulites: a metamorphic perspective. Geol Mag 126(3):215–331

Harlov DE (2000) Titaniferous magnetite-ilmenite thermometry and titaniferous magnetite-ilmenite-orthopyroxene-quartz oxygen barometry in granulite facies gneisses, Bamble Sector, SE Norway: implications for the role of high-grade CO_2-rich fluids during granulite genesis. Contrib Mineral Petrol 139:180–197

Harlov DE, Johansson L, Van den Kerkhof A, Förster H-J (2006) The role of advective fluid flow and diffusion during localized, solid-state dehydration: Söndrum Stenhuggeriet, Halmstad, SW Sweden. J Petrol 3–33

Hart SR, Dunn T (1993) Experimental Cpx/melt partitioning of 24 trace elements. Contrib Mineral Petrol 113:1–8

Hartel THD, Pattison DRM (1996) Genesis of the Kapuskasing (Ontario) migmatitic mafic granulites by dehydration melting of amphibolite: the importance of quartz to reaction progress. J Metamorph Geol 14:591–611

Hauri EH, Wagner TP, Grove TL (1994) Experimental and natural partitioning of Th, U, Pb and other trace elements between garnet, clinopyroxene and basaltic melts. Chem Geol 117:149–167

Hellebrand E, Snow JE, Mostefaoui S, Hoppe P (2005) Trace element distribution between orthopyroxene and clinopyroxene in peridotites from the Gakkel Ridge: a SIMS and NanoSIMS study. Contrib Mineral Petrol 150(5):486–504

Hill E, Wood BJ, Blundy JD (2000) The effect of Ca-Tschermaks component on trace element partitioning between clinopyroxene and silicate melt. Lithos 53(3–4):203–215

Hilyard M, Nielsen RL, Beard JS, Patiño-Douce A, Blencoe J (2000) Experimental determination of the partitioning behavior of rare earth and high field strength elements between pargasitic amphibole and natural silicate melts. Geochim Cosmochim Acta 64(6):1103–1120

Hölttä P, Paavola J (2000) P-T-t development of Archaean granulites in Varpaisjärvi, Central Finland. I. Effects of multiple metamorphism on the reaction history of mafic rocks. Lithos 50:97–120

Hölttä P, Huhma H, Mänttäri I, Paavola J (2000) P-T-t development of Archaean granulites in Varpaisjärvi, Central Finland. II. Dating of high-grade metamorphism with the U–Pb and Sm–Nd methods. Lithos 50:121–136

Horn I, Foley SF, Jackson SE, Jenner GA (1994) Experimentally determined partitioning of high field strength- and selected transition elements between spinel and basaltic melt. Chem Geol 117:193–218

Ionov DA, Hofmann AW (1995) Nb–Ta rich mantle amphiboles and micas: implications for subduction-related metasomatic trace element fractionations. Earth Planet Sci Lett 131:341–356

Irving AJ, Frey FA (1984) Trace-element abundances in megacrysts and their host basalts—constraints on partition-coefficients and megacryst genesis. Geochim Cosmochim Acta 48(6):1201–1221

Jacob DE, Foley SF (1999) Evidence for Archean ocean crust with low high field strength element signature from diamondiferous eclogite xenoliths. Lithos 48:317–336

Klein M, Stosch HG, Seck HA (1997) Partitioning of high field-strength and rare-earth elements between amphibole and quartz-dioritic to tonalitic melts: an experimental study. Chem Geol 138:257–271

Klein M, Stosch HG, Seck HA, Shimizu N (2000) Experimental partitioning of high field strength and rare earth elements between clinopyroxene and garnet in andesitic to tonalitic systems. Geochim Cosmochim Acta 64(1):99–115

Klemme S, Günther D, Hametner K, Prowatke S, Zack T (2006) The partitioning of trace elements between ilmenite, ulvospinel, annalcolite and silicate melts with implications for the early differentiation of the moon. Chem Geol 234(3–4):251–263

Leake BE (1997) Nomenclature of amphiboles: report of the subcommittee on amphiboles of the international mineralogical association, commission on new minerals and mineral names. Can Mineral 35:219–246

Luhr JF, Carmichael ISE (1980) The Colima Volcanic Complex, Mexico. Contrib Mineral Petrol 71:343–372

Luhr JF, Carmichael ISE, Varekamp JC (1984) The 1982 eruptions of El Chichón volcano, Chiapas, Mexico: mineralogy and petrology of the anhydrite-bearing pumices. J Volcanol Geotherm Res 23:69–108

Mahood GA, Stimac JA (1990) Trace-element partitioning in pantellerites and trachytes. Geochim Cosmochim Acta 54:2257–2276

Mänttäri I, Hölttä P (2002) U-Pb dating of zircons and monazites from Archean granulites in Varpaisjärvi, Central Finland: evidence for multiple metamorphism and Neoarchean terrane accretion. Precamb Res 118:101–131

Marchildon N, Brown M (2001) Melt segregation in late syn-tectonic anatectic migmatites: an example from the Onawa contact aureole, Maine, USA. Phys Chem Earth Part A 26:225–229

Martin H, Moyen J-F (2002) Secular changes in tonalite-trondhjemite-granodiorite composition as markers for the progressive cooling of Earth. Geology 30(4):319–322

McKenzie D, O'Nions RK (1991) Partial melt distributions from inversion of rare earth element concentrations. J Petrol 32:1021–1091

Nagasawa H (1970) Rare Earth concentrations in zircon and apatite and their host dacite and granites. Earth Planet Sci Lett 9:359–364

Nehring F, Jacob DE, Barth MG, Foley SF (2008) Laser-ablation ICP-MS analysis of siliceous rock glasses fused on an iridium strip heater using MgO dilution. Microchim Acta 160:153–163

Nehring F, Foley S, Hölttä P, van den Kerkhof A (2009) Internal differentiation of the Archean continental crust: fluid-controlled partial melting of granulites and TTG-amphibolite associations in Central Finland. J Petrol 50:3–35

Nicholls IA, Harris KL (1980) Experimental rare earth element partition coefficients for garnet, clinopyroxene and amphibole coexisting with andesitic and basaltic liquids. Geochim Cosmochim Acta 44:287–308

Nielsen RL, Gallahan WE, Newberger F (1992) Experimentally determined mineral-melt partition coefficients for Sc, Y and REE for olivine, orthopyroxene, pigeonite, magnetite and ilmenite. Contrib Mineral Petrol 110:448–499

Orejana D, Villaseca C, Paterson BA (2006) Geochemistry of pyroxenitic and hornblenditic xenoliths in alkaline lamprophyres from the Spanish Central System. Lithos 86:167–196

Paster TP, Schauwecker DS, Haskin LA (1974) The behaviour of some trace elements during solidification of the Skaergaard layered series. Geochim Cosmochim Acta 38(10):1549–1577

Patiño Douce AE, Beard JS (1995) Dehydration-melting of biotite gneiss and quartz amphibolite from 3 to 15 kbar. J Petrol 36(3):707–738

Patiño Douce AE, Harris N (1998) Experimental constraints on Himalayan anatexis. J Petrol 39(4):689–710

Pearce NJG, Perkins WT, Westgate JA, Gorton MP, Jackson SE, Neal CR, Chenery SP (1997) A compilation of new and published major and trace element data for NIST SRM 610 and NIST SRM 612 glass refernce materials. Geostand Newsl 21(1):115–144

Pfänder JA, Münker C, Stracke A, KM (2007) Nb/Ta and Zr/Hf in ocean island basalts—implications for crust–mantle differentiation and the fate of Niobium. ESPL 254:158–172

Pride C, Muecke GK (1981) Rare earth element distributions among coexisting granulite facies minerals, Scourian Complex, NW Scotland. Contrib Mineral Petrol 76:463–471

Prowatke S, Klemme S (2006) Trace element partitioning between apatite and silicate melts. Geochim Cosmochim Acta 70(17):4513–4527

Rapp RP (1995) Amphibole-out phase boundary in partially melted metabasalt, its control over liquid fraction and composition, and source permeability. J Geophys Res 100:15601–15610

Rapp RP, Shimizu N, Norman MD (2003) Growth of early continental crust by partial melting of eclogite. Nature 425:605–609

Ravindra Kumar GR (2004) Mechanism of arrested charnockite formation at Nemmara, Palghat region, southern India. Lithos 75:331–358

Rollinson HR, Windley BF (1980) Selective elemental depletion during metamorphism of archean granulites, scourie, Nw Scotland. Contrib Mineral Petrol 72(3):257–263

Rollinson HR (1979) Ilmenite-magnetite geothermometry in trondhjemites from the Scourian complex of NW Scotland. Mineral Mag 43:65–70

Rønsbo JG (1989) Coupled substitutions involving REEs and Na and Si in apatites in alkaline rocks from the Ilímaussaq intrusion, South Greenland, and the petrological implications. Am Mineral 74:896–901

Rudnick RL, Gao S (2003) The composition of the continental crust. In: Holland HD, Turekian KK, Rudnick RL (eds) The crust, vol 3. Treatise on Geochemistry. Elsevier-Pergamon, Oxford, pp 1–64

Rushmer T (1991) Partial melting of two amphibolites: contrasting experimental results under fluid-absent conditions. Contrib Mineral Petrol 107:41–59

Sage RP, Lightfoot PC, Doherty W (1996) Geochemical characteristics of granitoid rocks from within the Archean Michipicoten Greenstone Belt, Wawa Subprovince, Superior Province, Canada: implications for source regions and tectonic evolution. Precamb Res 76:155–190

Schnetzler CC, Philpotts JA (1970) Partition coefficients of rare-earth elements between igneous matrix material and rock-forming mineral phenocrysts; II. Geochim Cosmochim Acta 34(3):331–340

Schröter FC (2006) Mineral trace element distribution in amphibolite and granulite facies mafic rocks. Ph.D. thesis. The University of Sydney, Sydney, p 85

Schröter FC, Stevenson JA, Daczko NR, Clarke GL, Pearson NJ, Klepeis KA (2004) Trace element partitioning during high-P partial melting and melt-rock interaction; an example from northern Fiordland, New Zealand. J Metamorph Geol 22(5): 443–457

Schwandt CS, McKay GA (1998) Rare earth element partition coefficients from enstatite/melt synthesis experiments. Geochim Cosmochim Acta 62(16):2845–2848

Sen SK, Dunn T (1994) Dehydration melting of a basaltic composition amphibolite at 1.5 and 2 GPa: implications for the origin of adakites. Contrib Mineral Petrol 117:394–409

Sha LK, Chappell BW (1999) Apatite chemical composition, determined by electron microprobe and laser-ablation inductively coupled plasma mass spectrometry, as a probe into granite petrogenesis. Geochim Cosmochim Acta 63(22):3861–3881

Singh J, Johannes W (1996) Dehydration melting of tonalites. Part II. Composition of melts and solids. Contrib Mineral Petrol 125:26–44

Sisson TW (1994) Hornblende-melt trace-element partitioning measured by ion microprobe. Chem Geol 117:331–344

Sisson TW, Bacon CR (1992) Garnet/high-silica rhyolite trace element partition coefficients measured by ion microprobe. Geochim Cosmochim Acta 56:2133–2136

Sisson TW, Ratajeski K, Hankins WB, Glazner AF (2005) Voluminous granitic magmas from common basaltic sources. Contrib Mineral Petrol 148:635–661

Skjerlie KP, Johnston AD (1996) Vapour-absent melting from 10 to 20 kbar of crustal rocks that contain multiple hydrous phases: implications for anatexis in the deep to very deep continental crust and active continental margins. J Petrol 37(3):661–691

Skora S, Baumgartner LP, Mahlen NJ, Johnson CM, Pilet S, Hellebrand E (2006) Diffusion-limited REE uptake by eclogite garnets and its consequences for Lu–Hf and Sm–Nd geochronology. Contrib Mineral Petrol 152:703–720

Solar GS, Brown M (2001) Petrogenesis of migmatites in Maine, USA: possible source of peraluminous leucogranite in plutons? J Petrol 42(4):789–823

Springer W, Seck HA (1997) Partial fusion of basic granulites at 5 to 15 kb: implications for the origion of TTG magmas. Contrib Mineral Petrol 127:30–45

Stimac J, Hickmott D (1994) Trace-element partition-coefficients for ilmenite, ortho-pyroxene and pyrrhotite in rhyolite determined by micro-Pixe analysis. Chem Geol 117(1–4):313–330

Storkey AC, Hermann J, Hand M, Buick IS (2005) Using in situ trace-element determinations to monitor partial-melting processes in metabasites. J Petrol 46(6):1283–1308

Tiepolo M, Vannucci R, Oberti R, Foley S, Bottazzi P, Zanetti A (2000) Nb and Ta incorporation and fractionation in titanian pargasite and kaersutite: crystal-chemical constraints and implications for natural systems. ESPL 176:185–201

van Westrenen W, Wood BJ, Blundy JD (2001) A predictive thermodynamic model of garnet-melt trace element partitioning. Contrib Mineral Petrol 142(2):219–234

Vielzeuf D, Vidal P (ed) (1990) Granulites and crustal evolution. Kluwer, Dordrecht, p 600

Villaseca C, Romera CM, De la Rosa J, Barbero L (2003) Residence and redistribution of REE, Y, Zr, Th and U during granulite-facies metamorphism: behaviour of accessory and major phases in peraluminous granulites of central Spain. Chem Geol 200(3–4):293–323

Watson EB, Green TH (1981) Apatite/liquid partition coefficients for the rare earth elements and strontium. Earth Planet Sci Lett 56:405–421

White RW, Powell R (2002) Melt loss and the preservation of granulite facies mineral assemblages. J Metamorph Geol 20(7):621–632

Wilke M, Behrens H (1999) The dependence of the partitioning of iron and europium between plagioclase and hydrous tonalitic melt on oxygen fugacity. Contrib Mineral Petrol 137(1–2):102–114

Witt-Eickschen G, Harte B (1994) Distribution of trace elements between amphibole and clinopyroxene from mantle peridotites of the Eifel (western Germany): an ion-microprobe study. Chem Geol 117:235–250

Wolf MB, Wyllie PJ (1994) Dehydration-melting of amphibolite at 10 kbar—the effects of temperature and time. Contrib Mineral Petrol 115(4):369–383

Wood BJ, Blundy JD (1997) A predictive model for rare earth element partitioning between clinopyroxene and anhydrous silicate melt. Contrib Mineral Petrol 129(2–3):166–181

Wood B, Blundy J (2002) The effect of H_2O on crystal-melt partitioning of trace elements. Geochim Cosmochim Acta 66(20):3647–3656

Xiong XL (2006) Trace element evidence for growth of early continental crust by melting of rutile-bearing hydrous eclogite. Geology 34(11):945–948

Zack T, Brumm R (1998) Ilmenite/liquid partition coefficients of 26 trace elements determined through ilmenite/clinopyroxene partitioning in garnet pyroxenites. The 7th international kimberlite conference, pp 986–988

Zack T, John T (2007) An evaluation of reactive fluid flow and trace element mobility in subducting slabs. Chem Geol 239:199–216

Zack T, Foley SF, Jenner GA (1997) A consistent partition coefficient set for clinopyroxene, amphibole and garnet from laser ablation microprobe analysis of garnet pyroxenites from Kakanui, New Zealand. Neues Jahrbuch für Mineralogische Abhandlungen 172(1):23–41